Mustaffar A, Phan AN, Boodhoo K.

Hybrid heat pipe screw dryer: A novel, continuous and highly energy-efficient drying technology.

***Chemical Engineering & Processing-Process Intensification* 2018, 128, 199-215.**

Hybrid heat pipe screw dryer: a novel, continuous and highly energy-efficient drying technology

Ahmad Mustaffar*, Anh Phan and Kamelia Boodhoo

Process Intensification Group, School of Engineering, Merz Court, Newcastle University, NE1 7RU Newcastle upon Tyne, United Kingdom

*Corresponding author. Email: ahmad.mustaffar@newcastle.ac.uk

Abstract

We report on a novel type of screw conveyor dryer (SCD) with passive heating by an annular heat pipe, 'Heat Pipe Screw Dryer' (HPSD). It was firstly optimised, with its best performance corresponding to the lowest thermal resistances of 0.08–0.18 °C/W achieved at 11% filling ratio and in horizontal orientation. It was applied in the drying of a ceramic raw material slurry (initial moisture 33 wt. %). The highest moisture reduction of 46% (final moisture 18 wt. %) was achieved at 200°C and 260s. The specific moisture extraction rate (SMER) was 2.04 kg/kWh, more energy efficient than conventional dryers. Moreover, overall heat transfer coefficients were measured to be 35% higher than in a conventional steam jacketed-SCD due to the excellent thermal conductivity of the annular heat pipe. Solids build up on the surfaces increased from 3–62%, as moisture reduction increased from 10– 46%, respectively. Non-stick coating on the screw conveyor resulted in 10% fouling remediation on average. Significant potentials for even greater fouling reduction have been identified for this particular application of ceramic processing. Overall, the HPSD offers the opportunity for excellent energy recovery and space saving in drying processes, but more suitable for less fouling materials.

Keywords: screw conveyor dryer; annular heat pipe; ceramic processing; energy efficiency; process intensification

Research highlights:

- A hybrid technology of material conveyance and drying, termed as Heat Pipe Screw Dryer.
- The heat pipe was characterised to provide the best thermal performance.
- Highest moisture reduction of 46% obtained at 200^{o}C and 260s residence time.
- Energy efficiency was 2.04 kg/kWh, higher than most conventional dryers.
- Overall heat transfer coefficients were ~35% higher than a competing steam-SCD.

Nomenclature and abbreviations:

A	Area of heat transfer	m^2
Cp	Specific heat capacity	J/kg.K
Dsc	Outer diameter (OD) of the screw conveyor	mm
Dsh	Hollow shaft diameter of the screw conveyor	mm
dT or ΔT	Temperature differential	K
HPSD	Heat pipe screw dryer	
m	Mass	g
m_1	Mass in grams of the empty dish plus lid	g
m_2	Mass in grams of the dish plus lid plus test portion before drying	g
m_3	Mass in grams of the dish plus lid plus test portion after drying	g
$\dot{m}$	Mass flow rate	kg/s
P	Power	W
R	Thermal resistance	K/W
SMER	Specific moisture extraction rate	kg/kWh
T	Temperature	°C or K
Q	Heat transfer rate	W
U	Overall heat transfer coefficient	$W/m^2.K$

Subscripts:

f	Barrel space
in	Material remained
l	Liquid phase
l-lost	Liquid evaporated off a material
l-remained	Liquid remained in a material after evaporation
out	Material exited
s	Solid phase
T	Total
v	Vapour space

1 Introduction

It has been reported that drying constitutes up to 25% of industrial energy use in the developed nations [1]. With hundreds of dryer types available, the focus of innovation is in energy efficiency, reducing carbon footprint and thereby minimizing the impacts to the environment. Wang et. al [2] recently reviewed current developments in drying technology, which include impinging stream reactors [3], fluidised bed reactors [4], TORBED reactors [5], vertical thin film dryers [6], screw conveyor dryers [7] and microwave drying [8]. These technologies have highlighted the potential to improve the efficiency of drying by enabling shorter drying time, continuous processing as well as controlled and uniform drying i.e. uniform temperature distribution in the product.

Currently, in the ceramics industry, large volumes of water (~60 L) and high energy (~32 kWh) are consumed to produce one square metre of tile, in which the spray dryer has been identified as the main energy- and water-draining equipment. Therefore, it is of great interest to design an alternative, highly energy efficient continuous drying technology that would produce a similar product quality in terms of moisture content (5 – 7 wt. %), particle size distribution and porous granules in order to create a greener ceramics industry [9].

Jacketed screw conveyor dryers, an example of which is shown in Figure 1(a), have been investigated for the drying of fine crystalline solids [10], woodchips [11] and low rank coal [12], which demonstrate the flexibility for the screw conveyor in handling various types of materials i.e. from free-flowing powders to sticky, fibrous materials. A common heating media such as hot water, steam, pot oil, fused salt or Dowtherm oil [7] is pumped through a heat exchanger, thereby classified as ‘active’ heating. An alternative drying technique proposed in this paper is a novel type of screw conveyor dryer with

an annular heat pipe to dry the ceramic slurry. It is expected that by employing heat pipe as the dryer, it would help to reduce energy consumption in the ceramic drying process, as it has been demonstrated to benefit other applications like electronics and spacecraft cooling, heat recovery, etc. [13]. The annular heat pipe is a vacuum container with a fixed amount of 'working fluid', which does not require to be replenished for its entire operational lifetime. Hence, the annular heat pipe removes the need for auxiliary accessories or moving parts, in particular for the pumping of the heating media. Thus, it can be classified as a 'passive' and maintenance-free heating device.

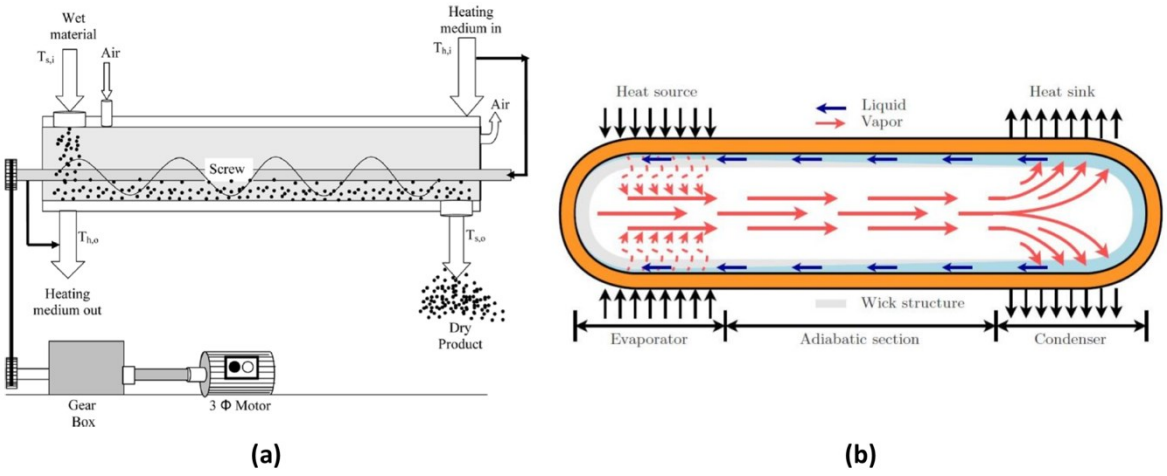

Figure 1. The Heat Pipe Screw Dryer is based on two technologies: (a) screw conveyor dryers [10] and (b) heat pipes [14]. The figures show a common configuration for both technologies.

Heat pipes transfer heat more efficiently and evenly than solid conductors due to their excellent effective thermal conductivities, which can range from 10 to 10,000 times (4,000 to 4,000,0000 W/m.K) the effective thermal conductivity of copper, depending on the length of the heat pipe [15]). Heat pipes generally consist of three distinct sections: the evaporator for heat input into the working fluid, the condenser for heat release from the condensate (Figure 1(b)) and the adiabatic section in between, where no heat exchange occurs with the environment. The fabrication of a heat pipe device involves firstly filling it with a pre-defined quantity of working fluid e.g. water, acetone, nitrogen, methanol, ammonia or sodium, depending on application and compatibility with the container

material. Vacuum condition is then created to lower its boiling point. Heat is absorbed at the evaporator by vaporising the working fluid. The vapour transports heat to the condenser region where the condensed vapour releases heat to a cooling medium. The condensed working fluid is returned to the evaporator by gravity (in thermosiphons) or by the heat pipe's wick structure, creating capillary action. A properly designed heat pipe is capable of maintaining near isothermal condition along its length, indicative of a negligible axial thermal resistance, as well as being highly responsive towards temperature fluctuations [16].

The main difference between the annular heat pipes and conventional heat pipes is that the cross-section of the vapour space in the former is annular instead of being circular (Figure 3 shows the cross-section of our investigated annular heat pipe), thereby the surface area for heat input and output can be significantly increased without increasing the outer diameter of the pipe [17]. This type of heat pipes is uncommon in literature but have been investigated as an isothermal furnace [18] and as a passive control of exothermic reactions [19]. Its use for the drying of conveyed slurry material is novel and therefore worthy of investigation.

In this work, the feasibility of employing such hybrid technology, termed as '**H**eat **P**ipe **S**crew **D**ryer', or HPSD, as an alternative for the spray dryer in ceramic processing is assessed. A novel continuous drying technology with device compactness leading to process intensification and energy-efficiency as its core operational principle has been developed and tested with the following objectives:

1. To characterize the operating conditions (filling ratio, inclination and temperature) for which the annular heat pipe gives the lowest thermal resistance between the evaporator and condenser, creating an excellent thermal conductor.
2. To study the drying of ceramic slurry under the optimum conditions obtained for the filling ratio and inclination of the annular heat pipe (see objective no. 1), in order to understand the

relationship between operational parameters, such as material residence time and heat pipe temperature, and process responses, such as moisture reduction and energy consumption.

2 Material and methods

2.1 Experimental rig design and set-up

Figure 2 shows the overview of the heat pipe screw dryer rig design containing a screw conveyor inserted inside an annular heat pipe. The important dimensional properties are shown in Figure 3 and 6. The screw conveyor had a total flighted length of 600 mm and both pitch and the outer diameter were 30 mm. The clearance between the screw and the barrel (inner wall of the inner tube) was 2.4 mm. It was constructed from 316-grade stainless steel to provide a good corrosion resistance in moist environment [20]. The screw was driven by a gear and motor assembly (Panasonic GV AC brushless motor) with a variable speed of 1 to 40 rpm and a resolution of 0.5 rpm.

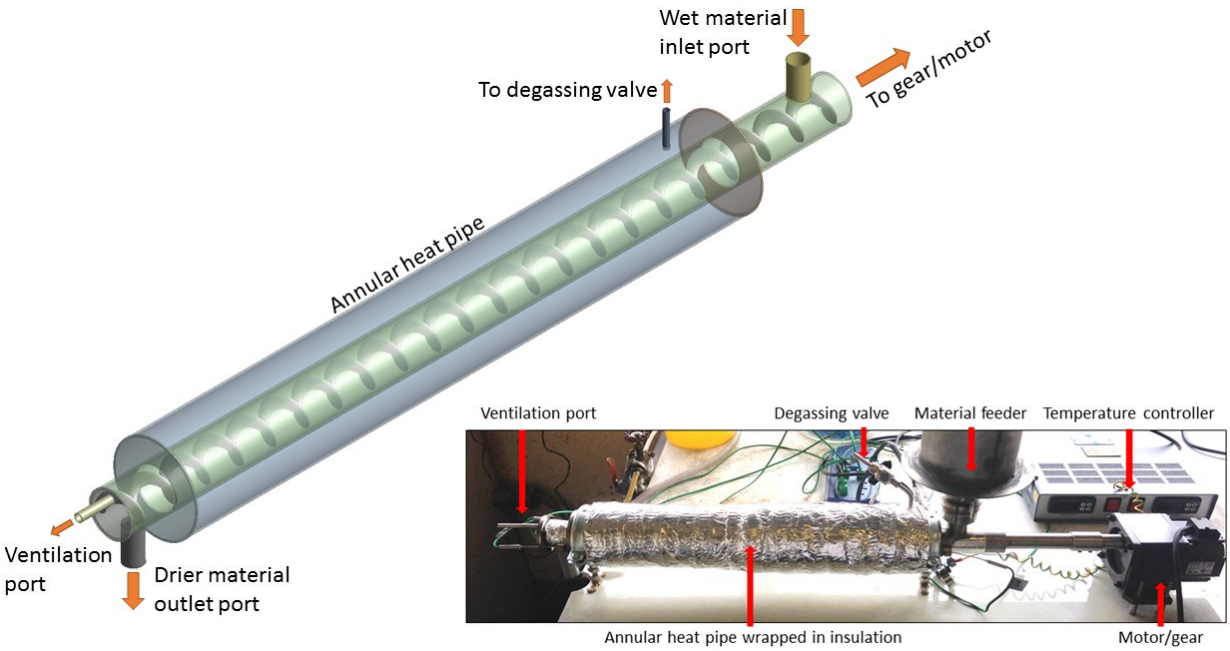

Figure 2. The overview of the heat pipe screw dryer (HPSD) showing the key design features. Note: the ventilation port also served as the hot swept air inlet port in some experiments.

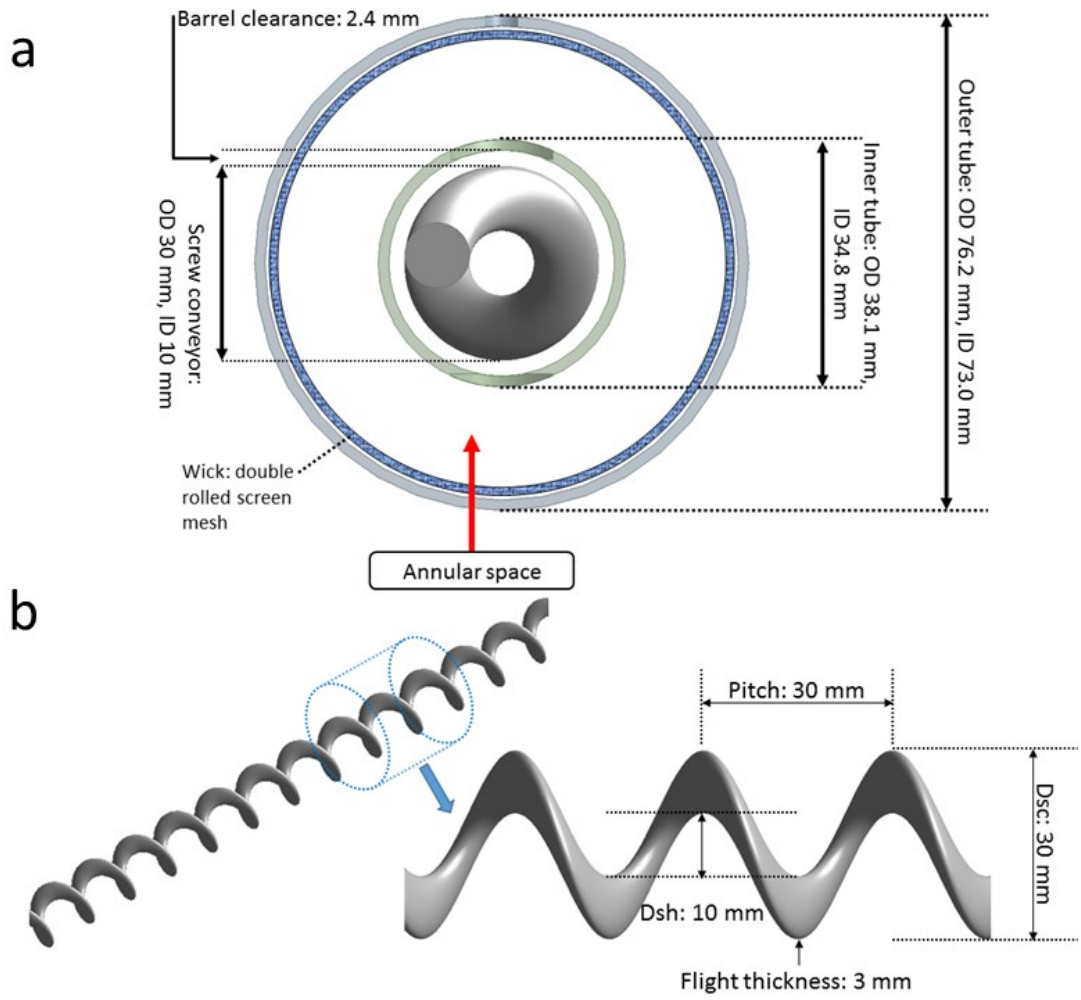

Figure 3. The key dimensions of the HPSD: (a) the cross-section and (b) a close up of the (hollowed) screw conveyor. Note: *Dsc* = screw outer diameter and *Dsh* = hollow shaft diameter.

The annular heat pipe was also constructed from 316-grade stainless steel. It was welded with end plates to create a vacuum-tight container. It contained a pre-defined amount of water as the working fluid, dependent on the selected filling ratio. Hydraulic pressure tests rated the vessel to be 40-bar proof (carried out in Thermacore, Ashington), which conformed to the recommended rating of 2.5x maximum saturated vapour pressure (for 200°C, 2.5*15.5 bar = 31 bar) [15]. Prior to the welding of the container components, a pre-cleaned and deoxidised stainless steel screen mesh (200 mesh size i.e. 200 pores per linear inch, double rolled) was spot-welded to the inner wall of the outer tube to function as a capillary wick, which would enable the condensate to return to the evaporator section from the condenser during the evaporation/condensation cycle. Spot welding ensured a close contact

with the wall, thereby maximizing thermal conductivity and minimizing local hot spots [21]. A degassing valve was welded to the outside of the outer tube to facilitate working fluid injection as well as to evacuate air via a pump to create a vacuum environment within the vessel. The working fluid used was deionized water due to its ease of handling and its proven operating temperature range of 1 to 325°C, as the range investigated in the HPSD experiments was 100 to 200°C [15]. A glass fibre heating tape (Electrothermal HT9, 244 cm length) was wrapped around the outer tube to create the evaporator section of 345 mm in length and the remaining length from 345 to 515 mm was designated as the condenser (Figure 4(a)). The evaporator therefore, constituted 67% of the overall length of the heat pipe and represents the first iteration of its size and the only one used in this paper. As a future work, the length would be varied as an experimental factor. As it was not applicable for the HPSD, no adiabatic section was specified. Type-K thermocouples (TC Direct, 1.5 mm diameter, accuracy: ±0.75%) were placed along the axial length of the outer tube surface (*TC-sX*) and inside the annular vapour space (*TC-vX*). Temperature was continuously recorded using a data logger (Picolog TC-08, accuracy: ±0.5°C or ±0.2%) and stored in a computer. Two thermocouples were placed inside the barrel space at each end of the evaporator and condenser (*TC-fX*) for the heat pipe characterisation study, which were subsequently removed prior to the moisture reduction study to enable the installation of the screw conveyor. Figure 4(b) shows the location of these thermocouples. To minimize heat loss to the environment, a three-layer fibreglass insulation (Fortaglas GW304, borosilicate E glass, 3mm thickness, thermal resistance: 20 m.K/W) was wrapped around the entire outer tube.

The start-up of the heat pipe involved injecting by a syringe through the degassing valve a pre-determined amount of water depending on the chosen filling ratio as an experimental factor (further discussed in Section 2.3.5). The air was drawn by a vacuum pump (KNF Neuberger VP Series, 0.3 bar) to create a vacuum environment. The heating was then switched on (at the controller) until a set

steady state temperature was reached. Temperature differentials along the axial length (surface, vapour space and barrel space) at steady state were then recorded for analysis.

The ventilation port was located at the end of the barrel (Figure 2). Its primary function was to provide a sufficient ventilation in order to remove the moisture created during the drying experiments, as recommended by Van den Hil, 2016 [22]. It was also used as an inlet or outlet for a hot air blower (Hakko FV310, 80°C, 0.15 m^3/min) as a heat augmentation in some experiments.

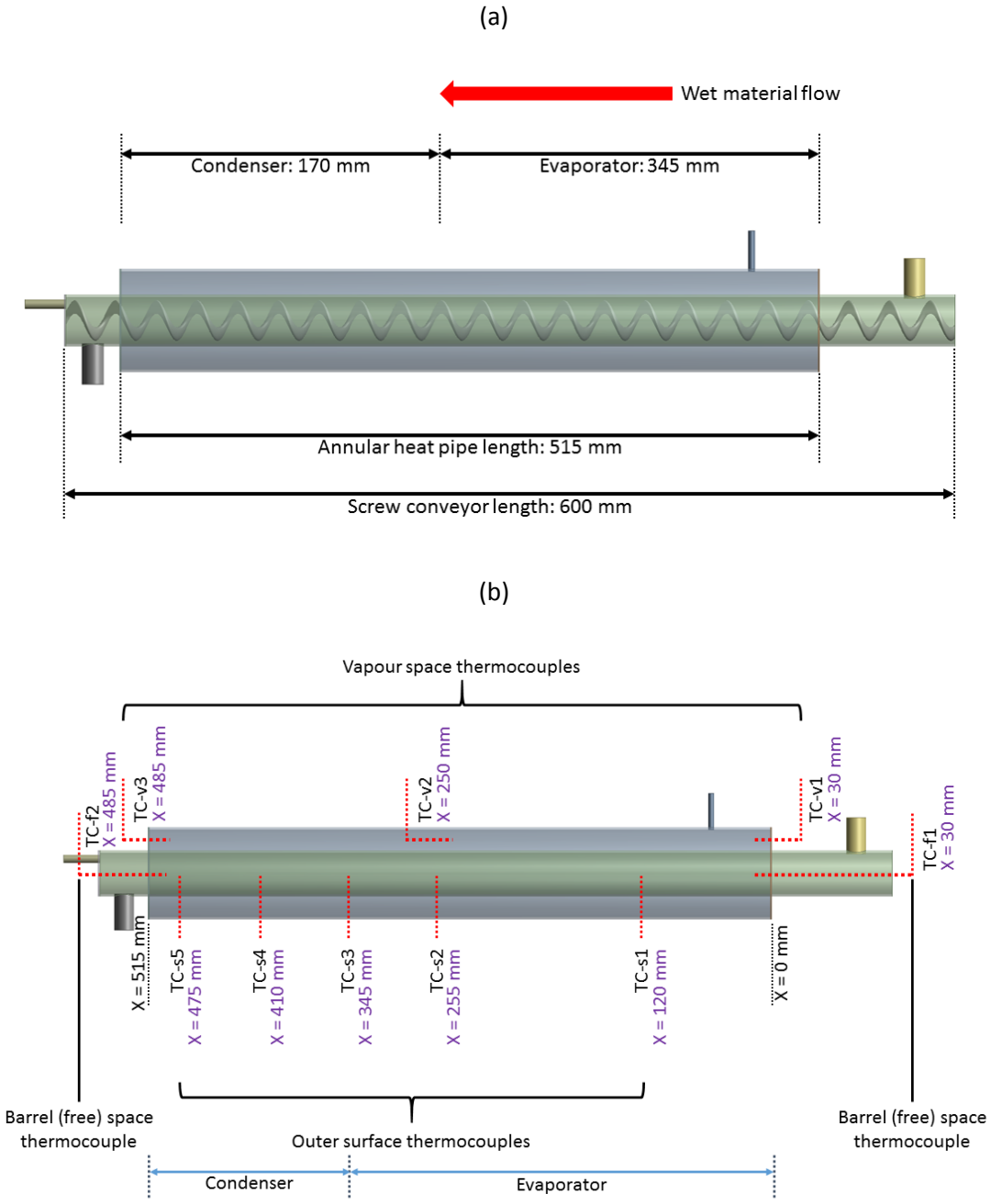

Figure 4. (a) The profile view of the HPSD showing the key dimensions of the annular heat pipe sections, (b) The location of the thermocouples in the set-up (the reference point, X = 0 mm, is the start of the evaporator section.

2.2 Ceramic slurry

The material processed in the HPSD was a ceramic raw material slurry from Euroatomizado, Spain (http://www.grupoeuroatomizado.com), normally processed in a spray dryer. The material arrived in batches with a median moisture content of 33 wt. % (wet basis). The solid components were a mixture of plastic clay, pheldpars, sands, caolin and dispersant as provided by the company. Figure 12(a) shows its original physical form prior to the drying process.

2.2.1 Tile press and analysis

The HPSD derived products that reached the target final moisture content of ≤ 7 wt. % were shipped to the laboratories of ITC (Instituto de Tecnologia Ceramica) in Valencia, Spain for tile pressing. The samples were assessed via microscope imaging and any constituent particles bigger than 1 mm were reduced in size to 500 µm particles. These particles were then pressed (under 250 kg/cm^2 pressure) into cylindrical test specimens (40 mm diameter, 7 mm thickness). These specimens were dried at 110°C in an oven with recirculating air. They were then weighed and the bulk density was determined by the mercury immersion method. After this, they were fired with a fast firing cycle (heating rate = 25°C/min) and a 6-min hold up at the peak temperature of 1100°C in an electric laboratory kiln. After firing, they were reweighed and the bulk density was measured. Firing shrinkage was evaluated as the difference between the dry and fired specimen diameter, on a dry weight basis.

2.3 Analysis

2.3.1 Moisture content

The moisture content was determined based on the method outlined in British Standard BS EN ISO 18134-3:2015 document for general analysis sample [23]. The moisture content of samples and the reduction in moisture were calculated based on Equation 1 and 2.

$$Moisture\ content\ (wt.\%) = \left(\frac{m_2 - m_3}{m_2 - m_1}\right) x\ 100 \quad \text{Equation 1}$$

$$Reduction\ in\ moisture\ (\%) \quad \text{Equation 2}$$

$$= \frac{Initial\ moisture - \ Final\ moisture\ (wt.\%)}{Initial\ moisture\ (wt.\%)}\ x\ 100$$

Where m_1 refers to the mass of the empty dish plus lid. m_2 and m_3 refer to the mass of the dish plus lid plus test portion before and after drying, respectively. All masses were measured in grams (g).

2.3.2 Residence time

Residence time refers to the time of particles/fluid spent in a control volume. In this study, the residence time was approximated by measuring the sample passing time in the barrel with the use of a digital timer (Cole Palmer Single Channel, accuracy: ±0.01%), as carried out in Kaplan and Celik [11]. The data were then used to compare with a model introduced by Fayed and Skocir[24], as indicated in Equations 3 and 4.

$$Required\ no.of\ revolution = \frac{Length\ of\ screw\ (mm)}{Length\ of\ pitch\ (mm)} \quad \text{Equation 3}$$

$$Residence\ time\ (s) = \frac{Required\ no.of\ revolution}{Rotational\ speed\ (rpm)} x\ 60 \quad \text{Equation 4}$$

Equation 4 indicates that the residence time is inversely proportional to the rotational speed. This is a very simplified model as it neglects material properties and characteristics e.g. powder, granular or slurry. It is also independent of temperature, barrel clearance size and barrel fill percentage, which all could impact the residence time independently or interactively.

2.3.3 Mass balance

A mass balance was primarily carried out to quantify the solids buildup (fouling), based on Equation 5 to Equation 8.

$$m_s + m_l = m_s + m_{l-remained} + m_{l-lost} \quad \text{Equation 5}$$

$$m_{l-lost} = m_l - m_{l-remained} \quad \text{Equation 6}$$

$$m_s + m_{l-remained} = (m_s + m_{l-remained})_{in} + (m_s + m_{l-remained})_{out} \quad \text{Equation 7}$$

$$Fouling\ (\%) = \frac{(m_s + m_{l-remained})_{in}}{m_s + m_{l-remained}} x\ 100 \quad \text{Equation 8}$$

Subscripts *s* and *l* are the masses of solid and liquid, *in* and *out* are the materials remained and exited, and *l-lost* and *l-remained* are the liquid evaporated off a material and the liquid remained in a material after evaporation, respectively.

2.3.4 Specific moisture extraction rate

For drying, an appropriate efficiency parameter is the specific moisture extraction (evaporation) rate (SMER) as defined by Mujumdar et al. 2009 [25] in Equation 9.

$$SMER\ (kg/kWh) = \frac{Amount\ of\ water\ evaporated\ (kg)}{Overall\ power\ consumption\ (kWh)} \quad \text{Equation 9}$$

Power consumption by both the heat pipe and screw conveyor was measured by the Energenie ENER007 Power Meter (accuracy: ±2%).

2.3.5 Heat pipe filling ratio

Heat pipe filling ratio describes the volume of working fluid present in the annular heat pipe per available unit volume of the evaporator, as defined in Equation 10. Based on the key dimensions of the heat pipe including the evaporator section length as shown previously in Figure 4(a), the volume of the evaporator was calculated as 1047 ml. Based on previous studies [26, 27], the filling ratio was recommended to be ~30%. Taking this value as the median with additional upper and lower values, three filling ratios were chosen: 11% (110 ml), 27% (280 ml) and 43% (450 ml).

$$Filling\ ratio\ (\%) = \frac{Volume\ of\ the\ working\ fluid\ (ml)}{Volume\ of\ the\ evaporator\ (ml)} x\ 100 \qquad \text{Equation 10}$$

2.3.6 Effective heat pipe thermal resistance

A heat pipe functions properly when the effective thermal resistance is low. It is defined as the overall heat pipe temperature difference at a given design power, which can be described in the following Equation 11 [21]. It takes into account the resistances due to conduction through the wall and wick, evaporation or boiling, axial vapour flow, condensation and conduction losses through the condenser's wick and wall [28].

$$Thermal\ resistance, R\ (°C/W) = \frac{T_{hot} - T_{cold}\ (°C)}{P\ (W)} \qquad \text{Equation 11}$$

Where *P* refers to the power input to the heat pipe, measured by the Energenie ENER007 Power Meter (accuracy: ±2%). T_{hot} and T_{cold} are the average surface temperatures of the evaporator (hotter region) and the condenser (cooler region), respectively. This parameter can also be expressed in (K/W).

2.3.7 Overall heat transfer coefficient

The overall heat transfer coefficient, *U*, refers to how well heat is transferred over a series of heat transfer media (or layers), through which conduction and/or convection occurs. It is represented in Equation 12.

$$U\ (Wm^{-2}K^{-1}) = \frac{Q}{A * \Delta T_{LMTD}} \qquad \text{Equation 12}$$

$$Q\ (W) = \dot{m} * Cp * \Delta T_{material} \qquad \text{Equation 13}$$

Where *Q* is the rate of heat taken up by the material (W). This parameter is not to be confused with the measured power, *P*, to the equipment, as *Q* refers to the measured energy uptake by the slurry material. $\dot{m}$ is the material flow rate (kg/s) fixed at 8.33 x 10^{-3} kg/s. $\Delta T_{material}$ is the temperature difference of the material (final – initial). *Cp* is the ceramic slurry specific heat (J/kg.K), assumed to be 920 J/kg.K. This specific heat value was assumed to be constant with temperature due to the lack of ceramic thermophysical data in literature [29]. *A* is the area of heat transfer, defined as the area of the inner surface of the inner wall (m^2) [7]. ΔT_{LMTD} is the logarithmic mean temperature difference between the medium (heat pipe) and the slurry.

2.4 Design of experiments

2.4.1 Experimental rigs

Two sets of geometrically identical rigs were manufactured in succession. The first rig was certified to operate only up to 150°C. However over time, the need to operate higher temperatures arose, therefore a second rig was manufactured with a better TIG (Tungsten Inert Gas) welding (Thornhill, Newcastle) and thus certified to operate at 40 bar maximum, a safe pressure threshold to operate up to 200°C. The same screw conveyor was used in both rigs in exception for the second rig, by which the screw was thinly coated (20 to 50 µm) with 'Xylan 1070 Black' (Bettablast, Shiremoor). The coating

contained composites of fluoropolymers and reinforcing binder resins that would reduce friction, improve wear resistance and provide non-stick properties [30]. Hence, this enabled a fouling remediation study to be conducted. The screw speed range is similar for both rigs: 1 – 40 rpm.

2.4.2 Experimental procedure

The procedure is summarized in Figure 5. For each experimental run, the heat pipe was started-up until it reached a steady state temperature. A 500.00 ± 0.05 g ceramic slurry was manually poured into the inlet port whilst the screw rotated at a set speed. While the drying process occurred, power to the heat pipe and screw conveyor were recorded and the temperature profiles were logged for analysis. The sample at the outlet was weighted and its moisture content analysed. At the end of the each test, a continuous flow of water was poured in until it ran clear in order to remove any solids build up and to prepare a clean barrel for the subsequent experimental run. The solids build up was recovered for fouling analysis.

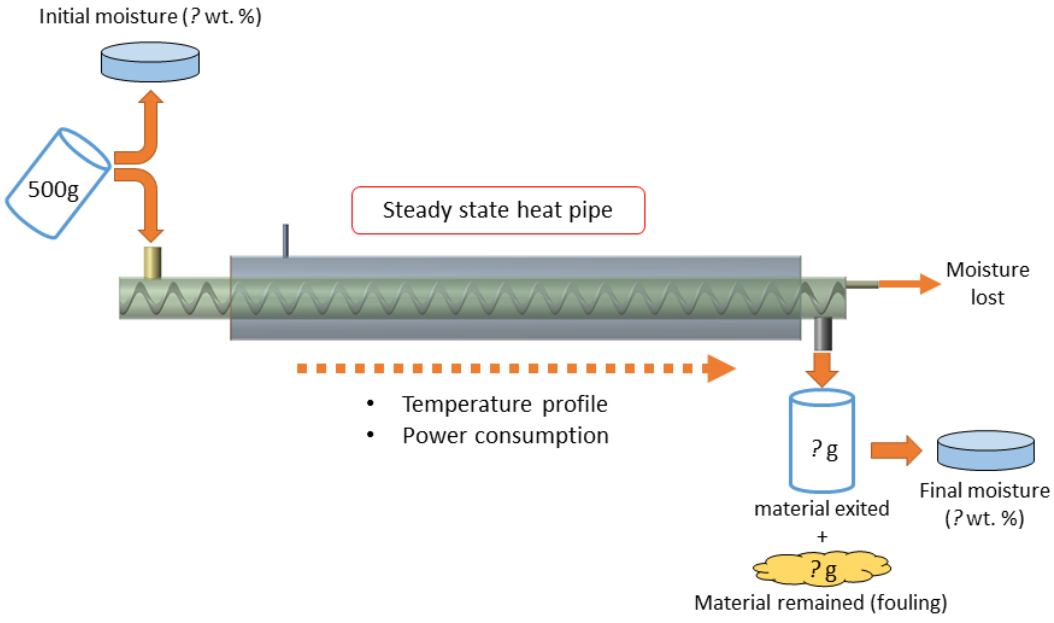

Figure 5. A graphical summary of the experimental procedure for the moisture reduction study.

2.4.3 Full factorial design

The experimentations were categorized into two sets, which were carried out in succession: 1) heat pipe characterisation and 2) moisture reduction of the ceramic slurry. The former was carried out in order to find optimised conditions from all factors that would result in the best heat pipe performance prior to the ceramic drying process. This is defined as the smallest thermal resistance along the axial length of the pipe, which is a function of the temperature differential between the evaporator and condenser sections: the smaller the value, the lower the resistance.

Three factors with three levels were investigated as shown in Table 1 and the response was the temperature differential (dT) between the evaporator and condenser sections in the 1) vapour space, 2) barrel space and 3) on the outer surface of the outer tube.

Table 1. High (+1), low (-1) and standard settings for the heat pipe characterisation study.

Factor	Low (-1)	Standard (0)	High (+1)
Filling ratio (%)	11	27	43
Inclination (°)	0 (Horizontal)	45	90 (Vertical)
Temperature (°C)	100	150	200

The moisture reduction experiments involved two independent, controllable factors: 1) heat pipe temperature and 2) screw speed, and residence time as a dependent, but observed factor (Table 2). Experimental responses were: 1) temperature differentials, 2) final product moisture content, specific moisture extraction rate (energy efficiency) and 3) fouling level.

Table 2. High (+1), low (-1) and standard (0s) settings for the moisture reduction study.

Factor	Low (-1)	Standard (0a)	Standard 2 (0b)	High (+1)
Heat pipe Temperature (°C)	100	150	175	200
Screw speed (rpm)	10	20	n/a	40
Material residence time (in seconds): uncontrollable, but observed factor				

Due to the identical geometry and specifications of the two fabricated rigs, experimental results were unified between both rigs. There were a few additional test runs:

- For Rig 1, for the 150°C heat pipe temperature, two screw speed levels were added: 2.5 and 5 rpm. For the extreme low speed of 2.5 rpm, a hot air heat augmenter (Hakko FV310, 80°C, 0.15 m^3/min, co-current) was used to further dry the slurry (refer Section 3.2.3). These additional runs were added to investigate whether the moisture reduction could be reduced further to result in the final moisture content of ≤ 7 wt. %, for direct tile pressing.
- For Rigs 1 and 2, 'long-term' tests to assess fouling on each of the non-coated and the Xylan-coated screws were carried out. This involved a continuous pouring of slurry for 1 hour at 150°C and 20 rpm (median settings). The screw was taken out in each case, left to dry under ambient conditions (12 hours) and the fouled materials were removed and weighed as dry mass.

Unless stated otherwise, all temperatures are referring to the heat pipe heater settings at the controller. The other temperature readings are referring to the heat pipe surface, vapour space or barrel space temperatures. Experiments were replicated three times for each set, for their reproducibility. Error propagation was applied whenever necessary. From analyses, the experimental uncertainties did not exceed 7.2%, which was acceptable (i.e. under 10%).

3 Results and discussion

3.1 Heat pipe characterisation study

It is known that a heat pipe functions properly when the overall thermal resistance is low [21]. Therefore, the main purpose of the heat pipe characterisation study was to find an optimum condition from three different factors i.e. heat pipe filling ratio, inclination and temperature in which the resulting temperature differential should be minimized. This would also allow for a greater understanding between the interplay of the aforementioned factors and the heat pipe performance. For simplicity, the following discussion involves mainly the vapour space temperature differential, dT_v = *TCv1 – TCv3* (for thermocouple locations, refer to Figure 4(b)) as the important processes of evaporation and condensation occur here. Analysis of variance indicated that among the three variables, the effects of filling ratio and inclination were significant (the significance cut-off was defined as $p < 0.05$) with $p = 0.000$ and 0.010, respectively. Whereas the effects of temperature was not, as $p = 0.290$. Therefore, the following discussion focuses on the former two factors for further simplication.

As shown in Figure 6, the trend for the barrel space temperature differential (dT_f = *TCf1 – TCf2*) indicates that it correlates well with that in the vapour space (dT_v), which can be attributed to the radial heat transfer from the vapour space to the barrel space. It also shows that the dT_v was reduced to negative values with the increase of both filling ratio and inclination. In other words, in some cases, the condenser was hotter than the evaporator, which was unusual for heat pipes. The reasons for this observation will be discussed later. The range of the dT_v was from -47.5 to 8.5K. The conditions that would provide smallest temperature difference were found to be 200°C, 11% filling ratio and fully horizontal i.e. 0° inclination (dT_v = 1.7K) whereas the adverse conditions correspond to 200°C, 43% filling ratio and fully vertical i.e. 90° inclination (dT_v = -47.5K).

Examination of the outer surface axial temperature is presented in Figure 7 for 11% filling ratio. It shows an isothermal condition from 345 to 475 mm. The distance from 0 to 345 mm was where the heating band was wrapped (evaporator), therefore the temperature here was higher. Heat input (in wattage) was a function of temperature setting: 272 W (100°C), 280 W (150°C) and 302 W (200°C). The profiles show that the temperature changed uniformly with the addition of power, therefore the annular heat pipe was operating satisfactorily [25 – 26].

Global thermal resistance of the annular heat pipe as a function of temperature evolution along the axial length of the wall was calculated and plotted in Figure 8. It shows that the resistance was smallest at 0.08°C/W (horizontal, 272 W) and largest at 0.31°C/W (inclined, 272 W). It also shows that the resistance changed slightly with changes in heat input. The resistance reduced slightly with heat input for the inclined and vertical orientations, whereas it increased slightly for the horizontal orientations. In general, thermal resistance in heat pipes should reduce greatly with heat input because higher heat input increases heat transfer effectiveness due to the improvement in nucleate boiling activity in the evaporator, which reduces thermal resistance in this region and hence, improving the overall resistance along the pipe. However, the effect is hard to observe in the annular heat pipe of present work because the heat input range investigated was relatively small at 30 W (272 to 302 W) compared to other works. This was because at 302 W, the vapour temperature already reached the vapour pressure safety limit and lower than 272 W heat inputs were deemed too small for useful CAHP operation as a continuous dryer. In general, the annular heat pipe of present work with 11% filling ratio performed within normal parameters at any angles and heat inputs investigated, because as a guideline, the global heat pipe resistances should be less than 1°C/W [27]. For experimental simplicity, the horizontal orientation was selected at 11% filling ratio, which gave 0.08 to 0.18°C/W resistance, for 272 to 302 W, respectively.

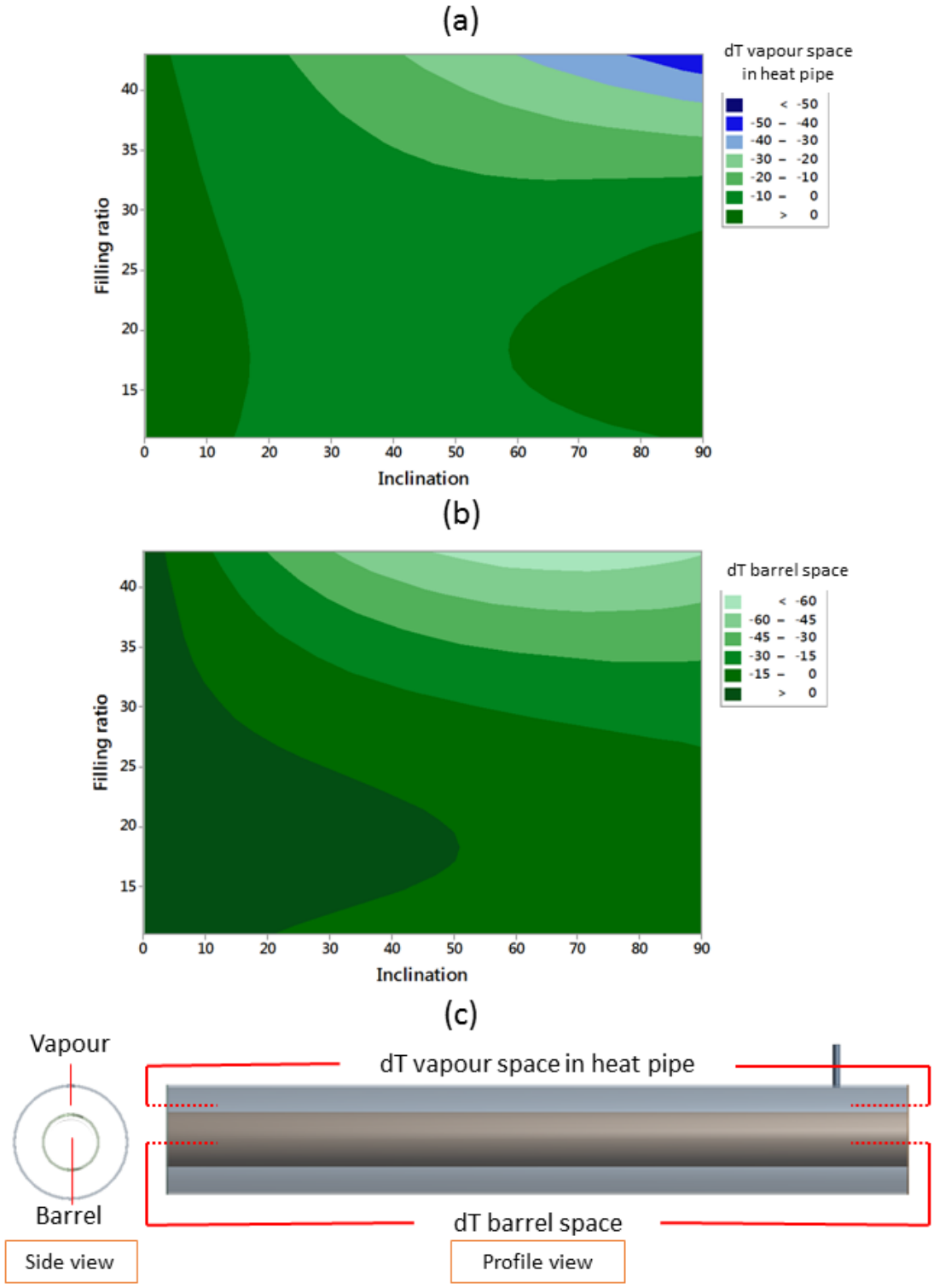

Figure 6. Contour plots for the effects of heat pipe filling ratio and inclination on the temperature differential between the evaporator and condenser sections for: (a) vapour space in annular heat pipe and (b) barrel space, (c) the locations where the temperature differentials were measured.

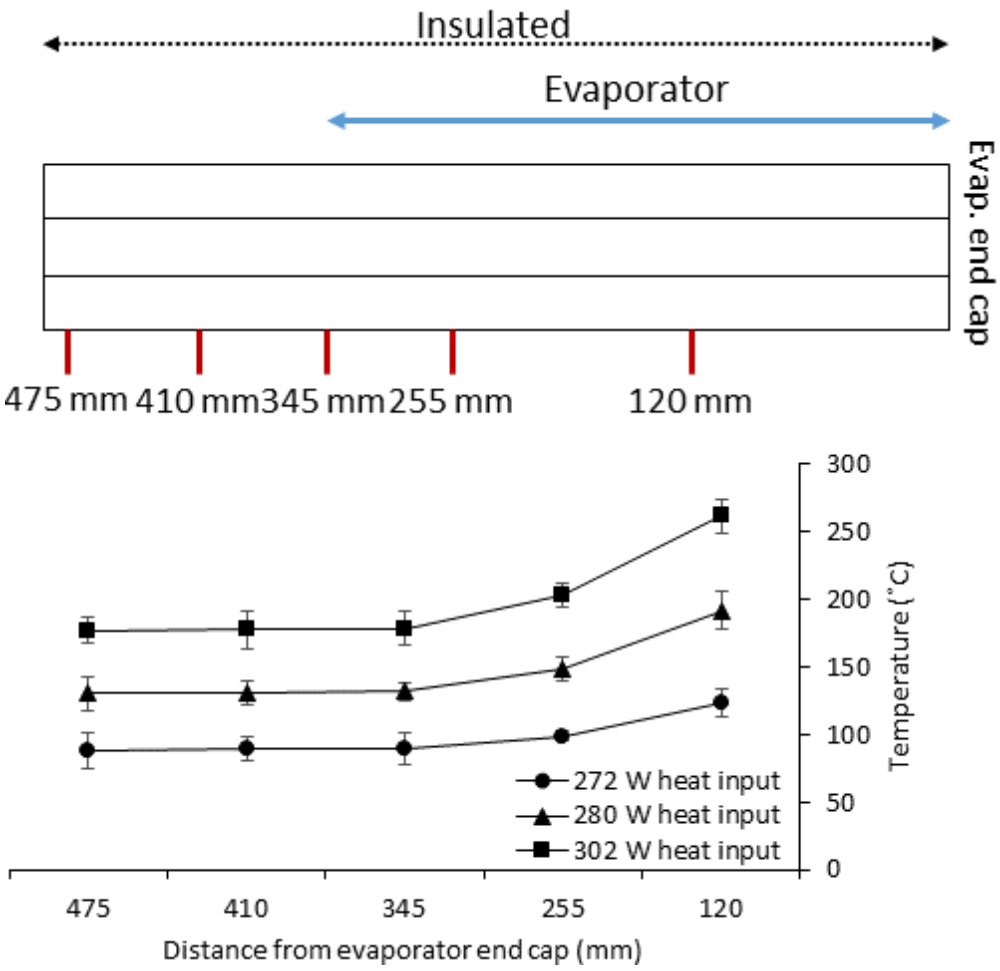

Figure 7. Axial temperature on the outer surface of the annular heat pipe. The distances indicated are relative to the evaporator end cap. Filling ratio at 11%.

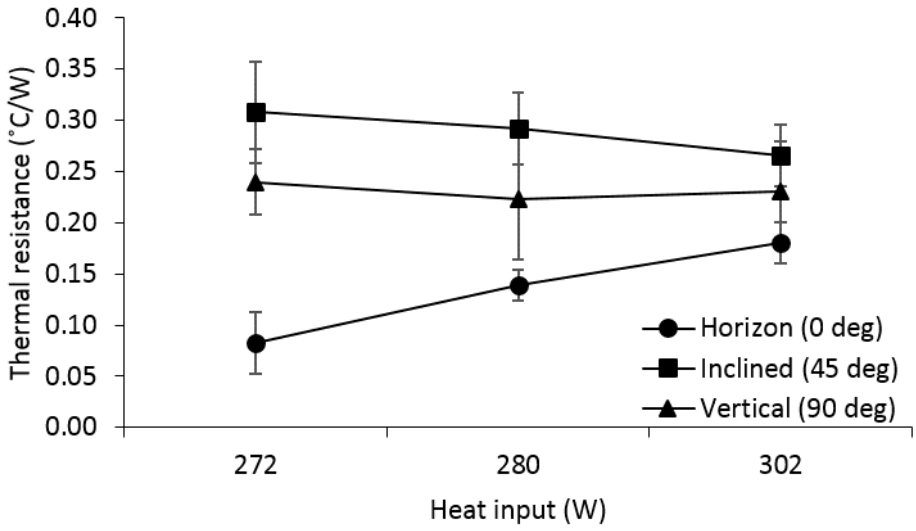

Figure 8. Steady state thermal resistance against power input to the heat pipe for the 11% filling ratio. Power input is a function of the heat pipe temperature setting.

The hotter condenser phenomenon could be due to the very thick layer of the working fluid at inclinations (45° – 90°), which was 38.2 mm (based on a simple calculation) for the fully vertical (90°) heat pipe. For the fully horizontal (0°) heat pipe, prior to heating, the water spread evenly along the bottom of the pipe, thereby only a thin layer needed to be heated and eventually the condensation/evaporation cycles occurred after a period of time. As the inclination was increased from 0° to 45° to 90°, the similar amount of water occupied the entire bottom portion of the pipe, instead of being spread out. The highest negative difference in temperature (dT_v = -48.0K) for the 43% filling ratio (Figure 9(a)) was indicative of this larger amount of water to be heated. From calculations, thermal resistance for the 38.2 mm water thickness was 6.0 x 10^{-2} K/W, whereas for the 3.2 mm stainless steel outer wall, 1.6 x 10^{-4} K/W. Due to this relatively low resistance along the outer pipe wall (R_{wall}/R_{water} = 0.003), the heat could have been prominently conducted to the condenser section via the wall over the evaporation process. For the 43% filling ratio, the evaporator of the fully vertical pipe (90^o) struggled to reach 115.0 ± 0.9K when its condenser had already reached 165.0 ± 1.2K at steady state. It implies that evaporation did occur, but the returned condensate replenished the huge volume of water that needed to be heated. Therefore, the evaporator thermocouple, TC-v1, was actually measuring the heated liquid phase, whereas the condenser thermocouple, TC-v3, was measuring the vapour phase (refer Figure 9(b)). While keeping the same filling ratio of 43%, but inclined at 45° angle, the dT_v was reduced from -48.0K to -29.3K. As the filling ratio was further reduced down to 11% while the heat pipe remained in a vertical position, the dT_v was substantially reduced to -1.7K. In comparison, the horizontal pipe temperature profile for 11% filling ratio shows a near isothermal condition (Figure 9(a)). It can be suggested that should it be necessary for the pipe to operate at an angle to increase the material residence time or for any other reasons, the filling ratio must be reduced to a minimum, feasible value, e.g. for the current HPSD, 11%.

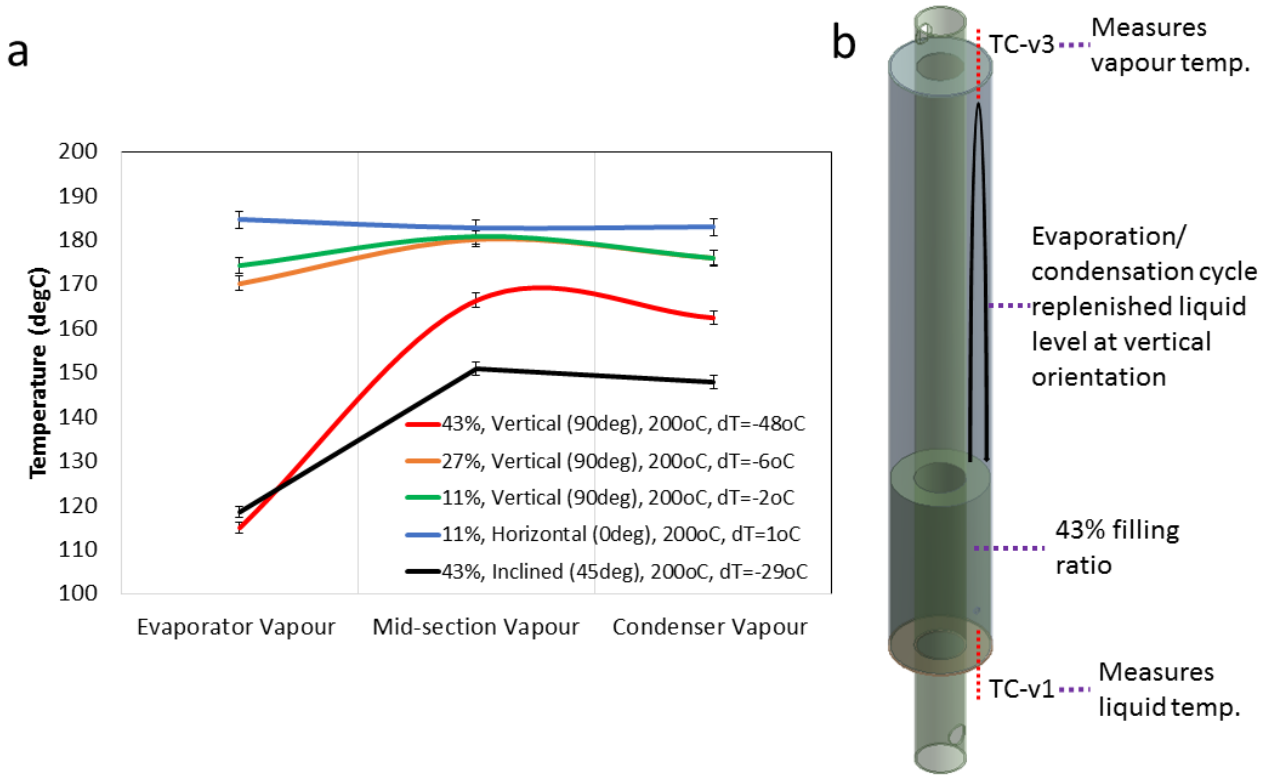

Figure 9. (a) Temperature profile at steady state along the heat pipe axial length in the vapour space for different filling ratios and at 200°C heat pipe temperature and (b) the phenomenon that occurred for the conditions of maximum filling ratio of 43% in a vertical inclination (90°).

3.2 Moisture reduction of the ceramic slurry

This study investigates the correlation between heat pipe temperature and screw speed on the material residence time (as an uncontrollable, but observed factor), moisture reduction of the slurry, energy efficiency and fouling. The optimized heat pipe conditions from the previous characterisation study were employed i.e. 11% filling ratio, horizontal configuration (0°) and at 200°C. A full tabulated data for the moisture reduction experiments can be found in Table 3.

The residence time is plotted against screw speed and temperature in Figure 10. The residence time was inversely proportional to the screw speed, as postulated by the model of Fayed and Skocir [24], presented in Equation 4. However, temperature also affected the residence time i.e. as the slurry

experienced higher moisture loss with increasing temperature, the material became more ‘cakey’ and more resistant to flow. At the smallest moisture reduction of 10%, the deviation from the model was 9% but, at the largest moisture reduction of 46%, the deviation was enormous at 116% (refer Table 3). This shows that this simplistic model cannot be used to describe the residence time in screw conveyor with an associated moisture loss process in the material conveyed, therefore a better model is desirable to be formulated.

Moisture reduction plotted in Figure 11 shows a progressive response when changes were made in the residence time and temperature. The smallest moisture reduction of 10% (final moisture content: 29.6 ± 3.8 wt. %) was obtained at the lowest residence time of 27.4 ± 2.2 s and temperature of 100°C, whereas the highest reduction of 46% (final moisture content: 17.8 ± 1.7 wt. %) was obtained at residence time of 260.0 ± 5.0 s and temperature of 200°C. Figure 12(b) shows the morphology of the product as a ‘pasty’ aggregate, which did not conform to the required size and moisture content for tile pressing. The maximum particle size for tile pressing is 500 µm, therefore a downstream size reduction equipment such as a roller compactor and milling (through screens) would be required

should the moisture content be reduced to the target level by any means possible e.g. by further increasing the temperature and residence time.

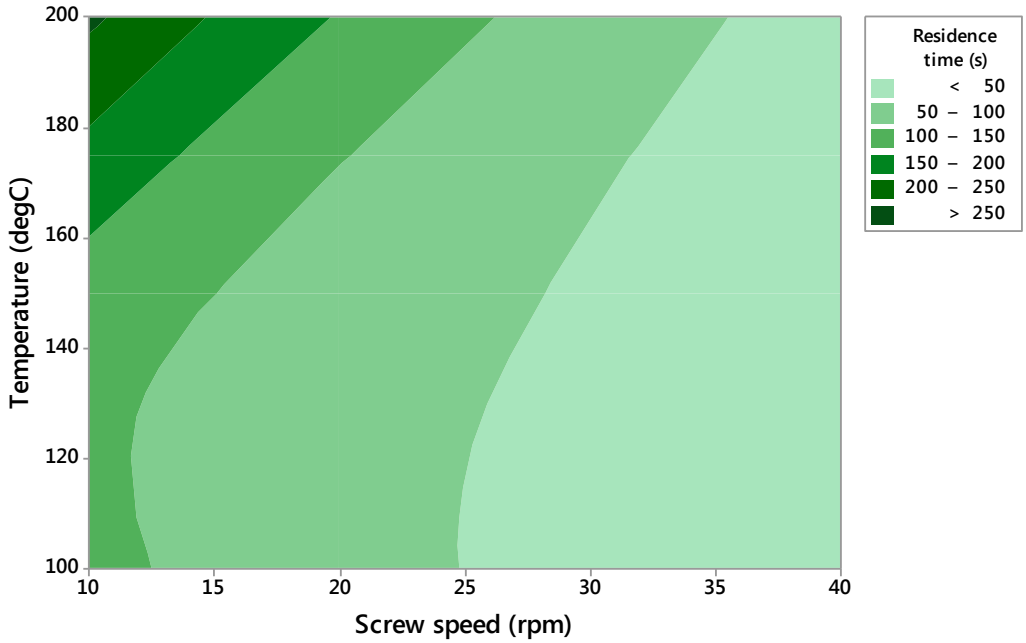

Figure 10. Material residence time (experimental) plotted against screw speed and heat pipe temperature.

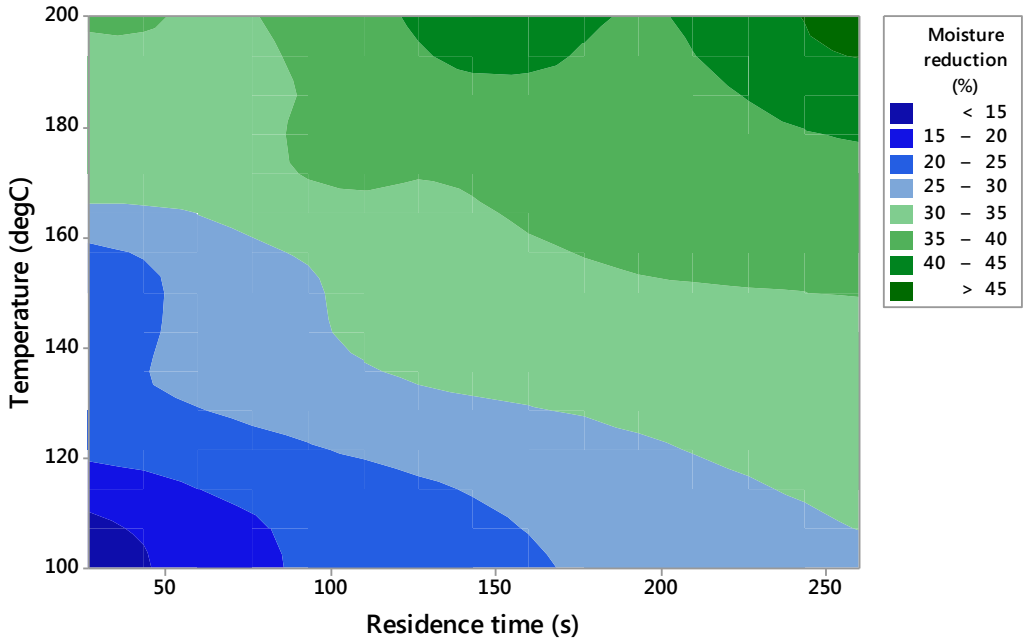

Figure 11. Moisture reduction plotted against material residence time and heat pipe temperature.

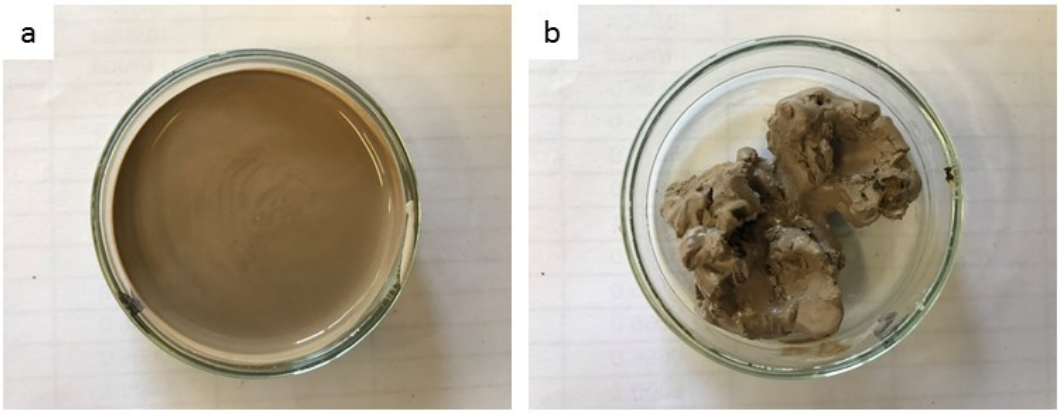

Figure 12. (a) The initial moisture content at 33 wt. %, (b) The material at 18 wt. % moisture content (wet basis), the lowest moisture content obtainable from the HPSD (at 260.0 ± 5.0 s residence time and 200°C temperature setting), showing a ‘pasty’ aggregate.

Table 3. Full results for the moisture reduction experiments

Process conditions		Residence time (s) [Model] *	Residence time (s) [Experimental]	Final moisture content (wt. %)	Moisture reduction (%)	SMER (kg/kWh)
Heat pipe temperature (°C)	Screw speed (rpm)					
100	40	30	27.41 ± 2.16	29.60 ± 3.75	10	0.45 ± 0.02
100	20	60	65.00 ± 2.10	27.04 ± 3.21	18	0.83 ± 0.05
100	10	120	116.00 ± 6.30	25.64 ± 3.38	22	0.94 ± 0.06
150	40	30	29.70 ± 0.95	26.16 ± 2.65	21	0.89 ± 0.07
150	20	60	76.85 ± 3.21	23.57 ± 1.78	29	1.11 ± 0.01
150	10	120	132.00 ± 5.66	21.91 ± 4.21	34	1.35 ± 0.16
175	40	30	32.08 ± 1.65	22.33 ± 2.18	32	1.44 ± 0.02
175	20	60	103.01 ± 5.21	21.05 ± 1.83	36	1.60 ± 0.31
175	10	120	186.00 ± 6.32	19.94 ± 1.79	40	1.75 ± 0.34
200	40	30	35.05 ± 1.49	21.33 ± 1.89	36	1.55 ± 0.05
200	20	60	146.53 ± 2.65	18.72 ± 2.84	43	1.91 ± 0.02
200	10	120	260.00 ± 4.95	17.74 ± 1.61	46	2.04 ± 0.07

*Based on a temperature independent-model by Fayed and Skocir, 1996 [24] (Equation 4).

3.2.1 Energy efficiency

An appropriate efficiency parameter for drying is the specific moisture extraction rate (SMER), which was defined in Equation 9 as the amount of water removed per unit of input power. Power was utilised to rotate the screw and to increase the temperature of the heat pipe. Power consumption is plotted against screw speed and heat pipe temperature in Figure 13(a) and (b), respectively. Both plots show that power increased linearly with screw speed and temperature. The maximum power consumption for all experimental conditions were 31.0 ± 0.5 W for the 40 rpm screw speed and 301.7 ± 7.7 W for the 200°C heat pipe temperature, showing that power consumption of the screw was only a fraction to that for the heat pipe: at most, only 10%. The SMER is plotted in Figure 13(c) against temperature and residence time. This trend is similar to the trend for the moisture reduction shown in Figure 11 because the SMER is proportional to the amount of water evaporated, as well as due to the linearity of the power consumption. Under the best conditions tested in this study, the efficiency was 2.04 ± 0.07 kg moisture removed/kWh (at 260.0 ± 5.0 s, 200°C), which was superior to conventional drying technologies including spray dryers (0.5 to 1.0 kg water removed/kWh) [25]. It was however, less efficient than steam compression dryers and heat pump dryers, reported to achieve 10.0 kg/kWh in certain conditions [31]. As no reports of SMER could be found for other screw conveyor dryers in the literature, a comparison between the HPSD and other conveyor dryers could only be made via the overall heat transfer coefficients as further discussed in Section 3.2.4. The HPSD's excellent energy efficiency can be attributed to the heat pipe efficiency as a thermal conductor, with very low thermal resistance at optimum conditions (as shown in Figure 8) as well as no pumping requirement of fluids compared to the active heating methods such as hot water, steam, oil, etc.

a

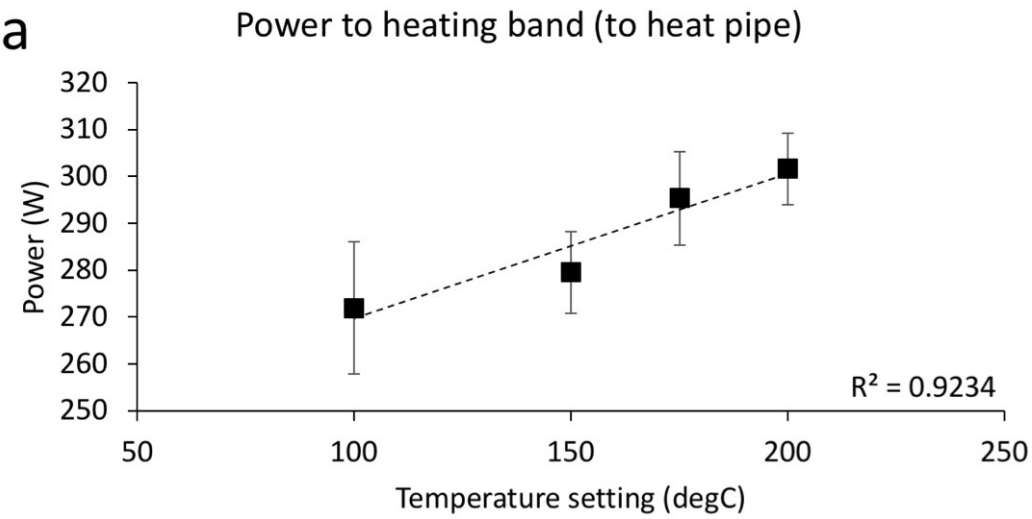
Power to heating band (to heat pipe)
Power (W)
320
310
300
290
280
270
260
250
50
100
150
200
250
Temperature setting (degC)
R² = 0.9234

b

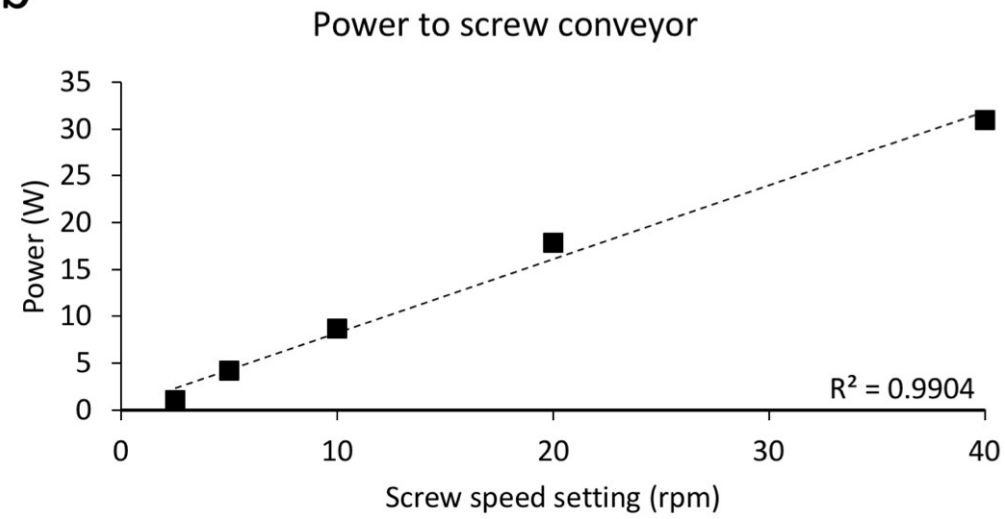
Power to screw conveyor
Power (W)
35
30
25
20
15
10
5
0
0
10
20
30
40
Screw speed setting (rpm)
R² = 0.9904

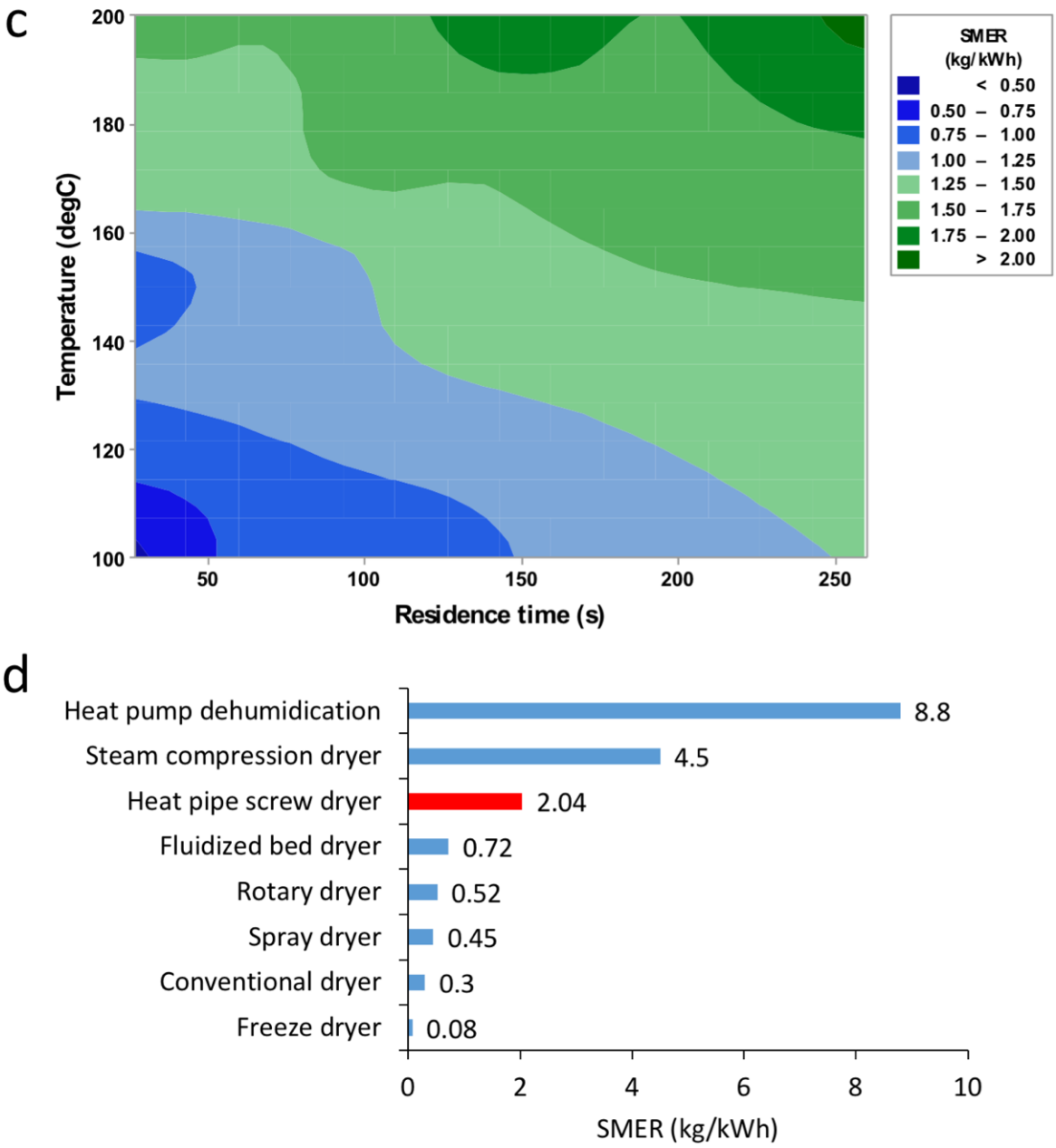

Figure 13. Power consumption plotted against level settings for: (a) heat pipe and (b) screw conveyor. (c) SMER plotted against residence time and heat pipe temperature and (d) energy efficiency for common drying technologies with the red bar indicating the HPSD (data from [25, 32]).

3.2.2 Fouling

The fouling was quantified in this work based on Equation 8. Two cases were investigated: (1) the non-coated screw (up to 150°C) and (2) the 'Xylan'-coated screw (up to 200°C). Xylan is a composite of fluoropolymers (PTFE, PFA and FEP), which is commonly used for friction reduction, wear resistance and non-stick application. It can also withstand operational temperatures up to 285K [30, 33]. The barrel, however, was not coated due to technical difficulty. It was found that fouling from 3 to 62%, as the moisture reduction was increased from 10 to 46%, respectively (Figure 14). Figure 15 shows its behaviour at different moisture conditions. At lower moisture reductions (Figure 15(b)), the slurry was still mobile as it had an ample amount of moisture to move through the barrel and was easily conveyed by the screw. As the moisture was further removed, the slurry became 'cakey' and stuck to the surfaces of the barrel wall mainly (Figure 15(c)). Figure 15(d) shows an extreme solids buildup on both the barrel wall and screw after a long-term test (1-hour continuous operation, 150°C, 20 rpm). The maximum thickness of this fouled layer could be roughly estimated as the clearance between the screw and the barrel. In continuous processing, this fouled layer would present an added thermal resistance, causing heat transfer inefficiency as well as material loss. A simple solution would be to reduce the clearance to a bare minimum e.g. 0.0 – 0.5 mm, so that as it rotates, the screw would scrape this layer off as it starts to buildup. A design guideline by Waje et al., 2007 [7] mentioned that the recommended clearance is 1.5x the size of maximum particles to be processed, to prevent the material jamming the machine and the loss of energy, but this is only applied for powders or crystalline materials, and not slurry-type material.

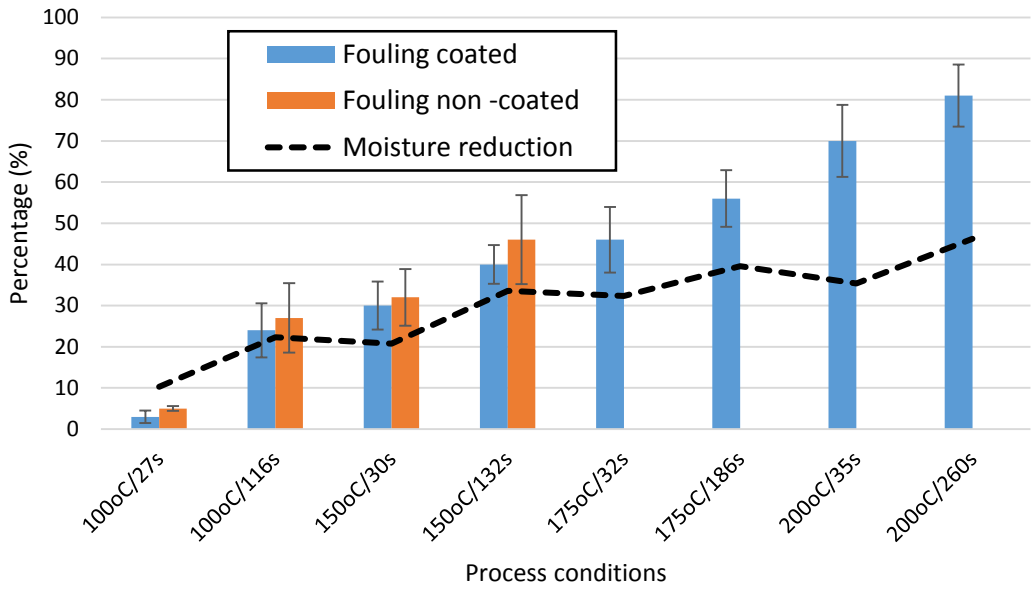

Figure 14. Fouling (in %) for the coated and non-coated screws, plotted against process conditions: residence time and temperature. Moisture reduction (in %) is plotted as the dotted line for reference.

It is also apparent from the plot in Figure 14 that the coating on the screw had little impact upon fouling remediation. On average for all experimental conditions, the overall fouling was only reduced by 10% despite the fouling on the coated screw being reduced by 55% compared to the non-coated screw (Figure 16). This unexceptional remediation can be attributed to the non-coating of the inner barrel wall where most of the solids build up occurred as shown in Figure 15(d). This suggests that the overall solids build up could have been reduced significantly if the wall was coated. This coating would not impact upon heat transfer performance i.e. added resistance layer between heat pipe and material, as the thermal resistance from this coating (PTFE conductivity: 0.25 W/m.K [34]) would be minimum because only 20 – 50 µm coating thickness would be applied. After each experimental run, water at room temperature was poured through the barrel continuously while the heat pipe and the screw were still operating (to aid the cleaning process) until the exit water was satisfactorily clear. This was carried out to dilute and leach off any solids build up to prepare for the next experimental run. Figure 15(a) shows that despite this exercise, there were still some solid residues on the barrel and

screw surfaces. Therefore, it is recommended that a better, inexpensive solvent e.g. acetone or alcohols should be used as a substitute to the water wash or a high-pressure jet water wash could be implemented.

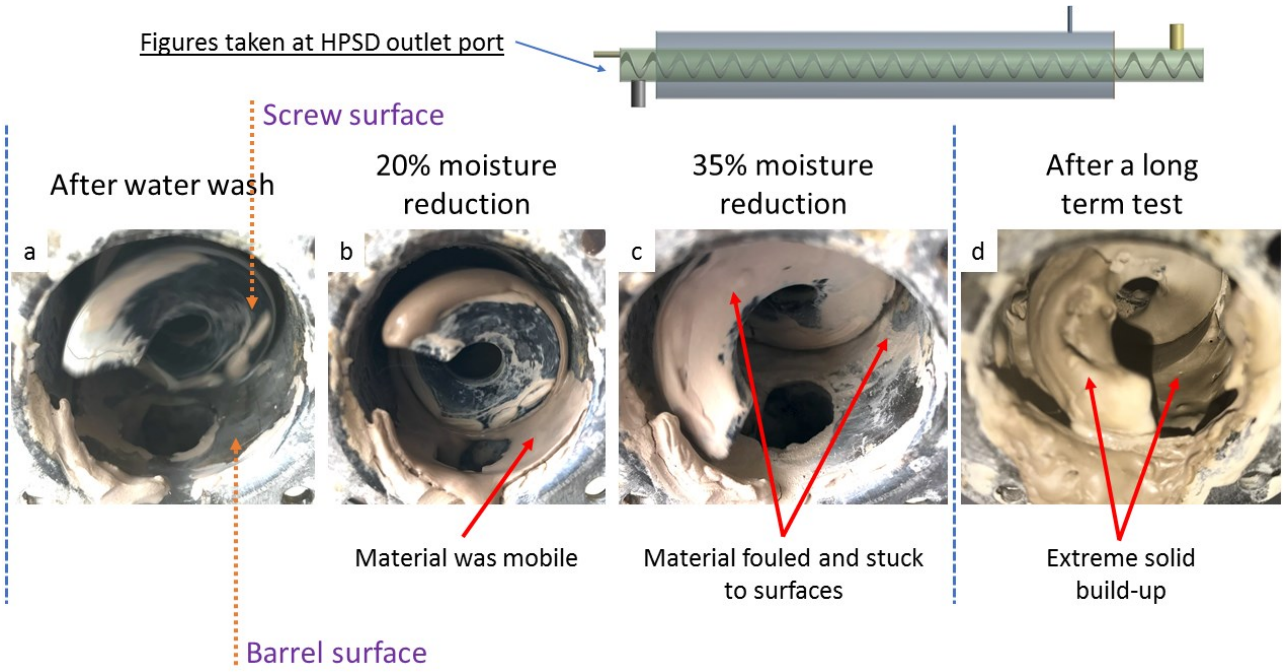

Figure 15. Solids buildup in the HPSD (side view of the HPSD at the outlet): (a) after a thorough water clean-up, showing residuals on the surfaces, (b) at 20% moisture reduction, (c) at 35% moisture reduction and (d) after a long-term test (shown only for the non-coated screw: for comparison of the coating conditions, refer Figure 16).

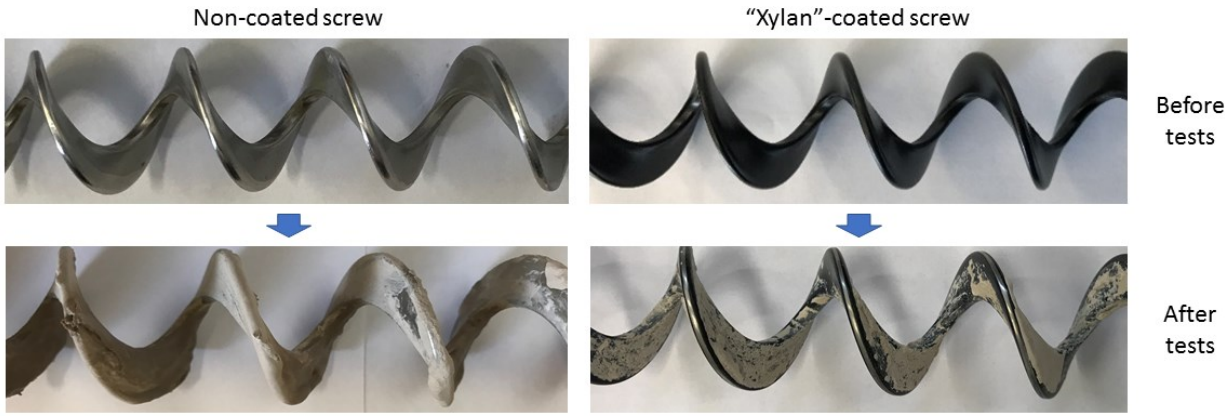

Figure 16. The screw was diassembled after a long term test (median settings: 150°C, 20 rpm for 1h duration) for the non-coated screw and the 'Xylan'-coated screw.

3.2.3 Extreme conditions carried out in the first rig and with a heater blower

In the first rig where the temperature was limited to 150°C, the maximum moisture reduction obtained was 34%, corresponding to 21.9 ± 4.2 wt. % final moisture content for 150°C temperature and 132.0 ± 5.7 s residence time. In order to further reduce the moisture to the target final level of ≤ 7 wt. % for direct tile pressing, the residence time was increased by reducing the screw speed to 2.5 rpm (530.0 ± 5.8 s residence time) and with the additional aid of a hot air blower (Hakko FV310, 80°C, 0.15 m^3/min, co-current flow), the moisture was further reduced to 75%, equivalent to 7.1 ± 1.0 wt. % final moisture content. This however, occurred at the expense of heavy fouling and energy penalties as the fouling exceeded 86% (Figure 17(a)) and the energy efficiency was greatly reduced from 1.35 ± 0.16 to 0.56 ± 0.01 kg/kWh due to the high energy consumption of the heater blower. The air flow was alternated between counter- and co-current, but the latter was found to be more effective as it aided the removal of the dried product from the barrel formed as a result of the heavy caking at the extremely low rotation of 2.5 rpm. Figure 17(b) shows the product at 7.1 ± 1.0 wt. % moisture content, which was carefully packed and shipped to the ITC Laboratories in Valencia, Spain for tile pressing. This procedure was already described in Section 2.2.1. The samples had to be remoistened in ITC due to some moisture loss during shipment. With the samples being non-spherical and with a global size of > 1 mm (Figure 17(c)), they did not conform to the requirements for ceramic processing and had to be milled to particles less than 500 µm in size. Cylindrical tile samples were then pressed and fired in a kiln (Figure 17(d)). Analysis was carried out and the results are shown in Figure 17(e). The low shrinkage value of 10% (< 10% as an industrial guideline) under 1100°C temperature meant that tile had a great dimensional stability [35, 36].

Due to the heavy penalties imposed by this method, the conditions were not repeated in the second rig. In addition, the non-conformity of the dried product's morphology implied that an additional ceramic size reduction process downstream was necessary. Overall, these factors were disadvantageous to the development of a compact and energy-efficient drying technology and further tests with the air stream were therefore not pursued.

(a)

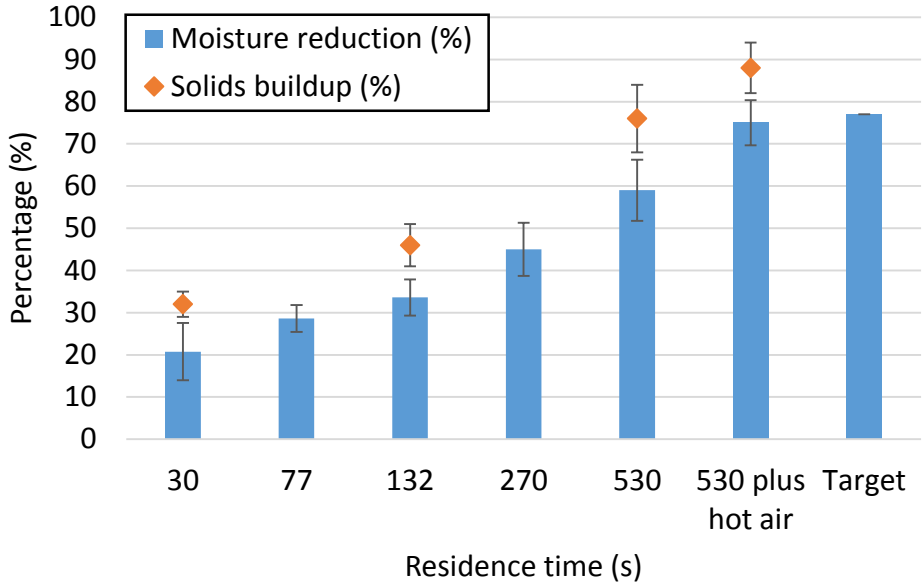

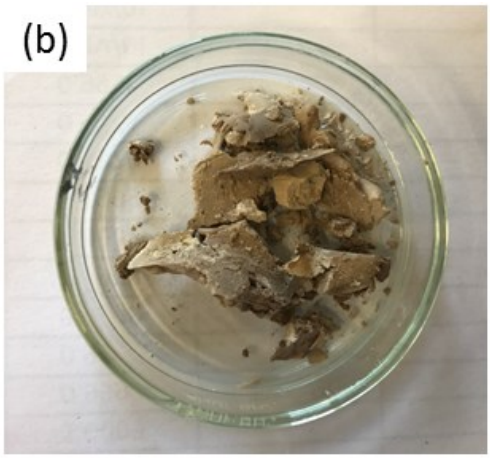

(e)

Variables	HPSD sample
Moisture content (%)	5.5
Pressing pressure (kg/cm^2)	250
Bulk density pressed sample (g/cm^3)	1.966
Firing temperature (°C)	1100
Bulk density fired sample (g/cm^3)	1.769
Firing shrinkage (%)	10

Figure 17. Extreme conditions experiments were carried out in the first rig: (a) moisture reduction and fouling (%) as a function of residence time, (b) the 7 wt. % moisture content product, (c) microscope imaging of crushed and dried HPSD product, (d) the pressed cylindrical tile specimens heated at 1100°C and (e) the tabulated data of the 'dry to fired' specimens' results.

3.2.4 Heat transfer analysis

The temperature profiles logged along the heat pipe surface as well as inside the vapour space are beneficial in understanding the mechanism of heat transfer from the annular heat pipe to the material. The outer heat pipe surface temperatures, logged by thermocouples *TC-s1* to *TC-s5* in Figure

18(a – c) (refer Figure 4(b) for the thermocouple locations) indicate that as an overview, a normal heat pipe operation of a higher evaporator temperature and a lower condenser temperature occurred i.e. the evaporation and condensation cycle occurred as predicted. With the presence of the ceramic slurry, as it being conveyed through the barrel (labelled as the "With load" profiles), temperature changes were observed along the axial length of the pipe: this was observed for all cases (the plots here are only for 100 – 200°C, 40 rpm (260 s residence time), for demonstration purposes). This means that the condensation process, whereby the heat was being transferred from the vapour space, through the barrel wall and towards the material, already started to occur at the start of the heat pipe i.e. the evaporator section. For the 100°C case, the dT_s (i.e. the differential temperature on the heat pipe outer surface) between the "No load" and the "With load" conditions at the start of the evaporator section (*TC-s1*) was 3.8K, whereas at the end of condenser section (*TC-s5*), the dT_s was 19.3K. Whereas for the 200°C case, the dT_s between *TC-s1* and *TC-s5* for both "No load" and "With load" conditions were 22.1K and 37K, respectively. These indicate that the operation fit the criteria of a normal heat pipe i.e. the heat discharge to a cooling medium (in this case, the slurry) occurs more prominently at the condenser. However, it is more interesting to examine the conditions in the vapour space, where the important processes of evaporation and condensation took place.

Figure 18 also plots the vapour space temperature profiles (data from thermocouples *TC-v1 – 3*). Here the temperature differentials, dT_v (i.e. in the vapour space), were observed to be almost uniform for both "No load" and "With load" conditions at both heat pipe sections, albeit a slight higher in magnitude in the condenser section. The data indicate that condensation clearly occurred on the inner barrel surface, which was in close contact with the slurry, along the axial length of the heat pipe. Thereby, it is suggested that the heat transfer of the latent heat energy from the condensed vapour to the conveying ceramic slurry took place all along the heat pipe length, not just at the designated 'condenser' section.

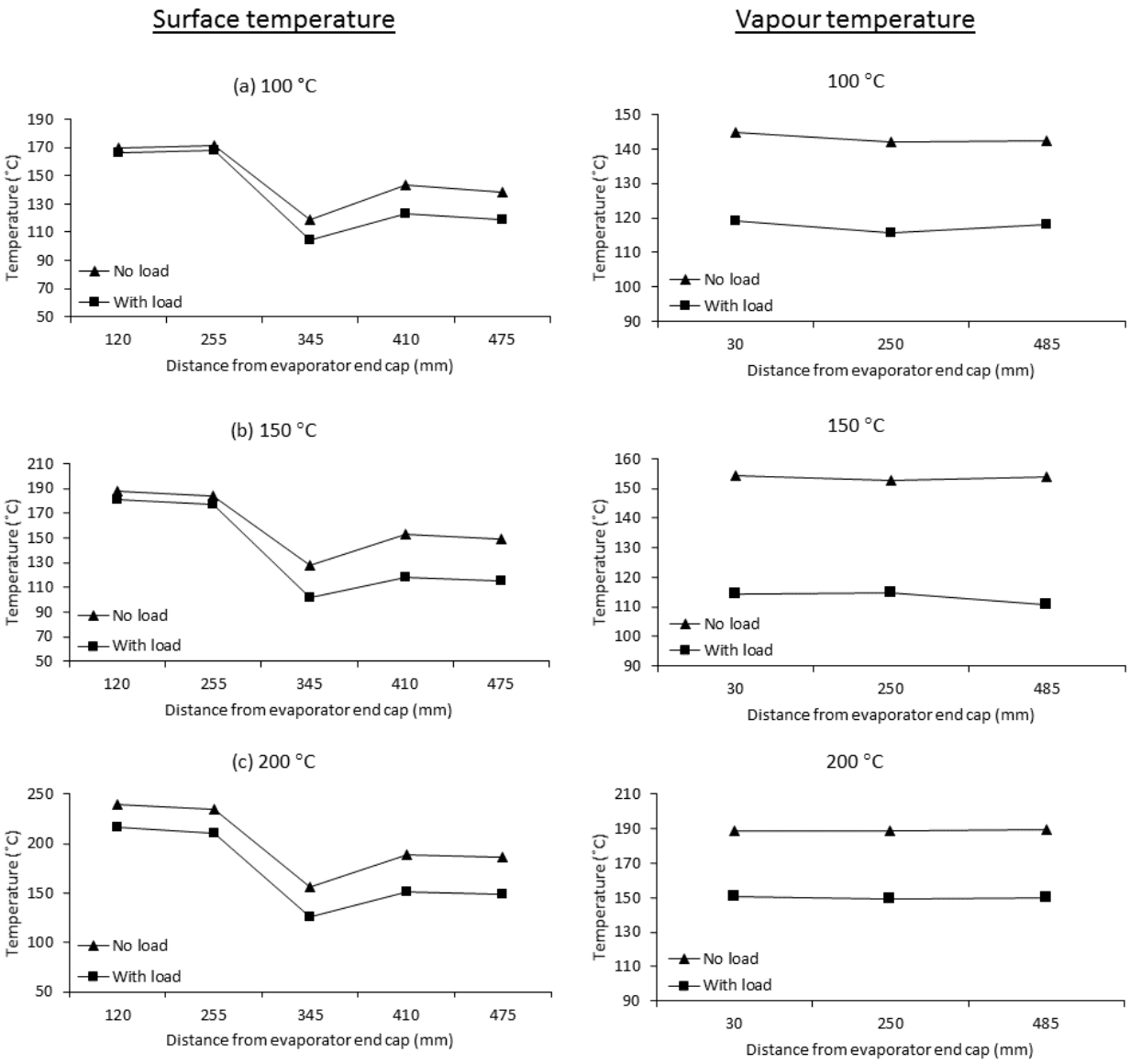

Figure 18. Temperature profiles of the heat pipe outer surface and the vapour space for: (a) 100°C, (b) 150°C and (c) 200°C (all at 40 rpm rotational speed, 11% filling ratio and horizontal) for the "No load" and "With load" conditions.

The overall heat transfer coefficient, *U*, is an important parameter to quantity the indirect heat transfer to the material ('indirect' i.e. the transfer of heat from the heating medium to the cooling material is done through heat transfer barriers, including the fouled layer. This parameter is dependent on the specific heat (Cp) of the material. The earliest reported *U* values for the screw conveyor dryers indicate values in the range of 6 – 70 $W/m^2.K$ [37]. More recently, Waje et al. 2006 [10] have studied the thermal performance for a steam-jacketed screw conveyor in drying fine white

crystalline material and reported the values of 46 – 102 W/m^2.K for moisture reduction in the range of 13 – 92%. The *U* values from this recent study are plotted in Figure 19 alongside with the HPSD data. It shows that in general, the *U* value increases with the increase of moisture reduction, which is a function of the heating temperature and residence time in both studies. Within the comparable moisture reduction range, the *U* values for HPSD are 35% higher on average, from 10 to 46% moisture reduction. These data demonstrate that the annular heat pipe is an excellent heating medium for screw conveyor dryers, in addition to being a promising drying technology. Should the fouling layer be remediated, the values would be further improved. It would also be interesting to continue the moisture reduction (up to 90%) through increasing the levels of current factors namely, temperature and residence time, in order to provide a full comparison with this work of Waje et al. 2006.

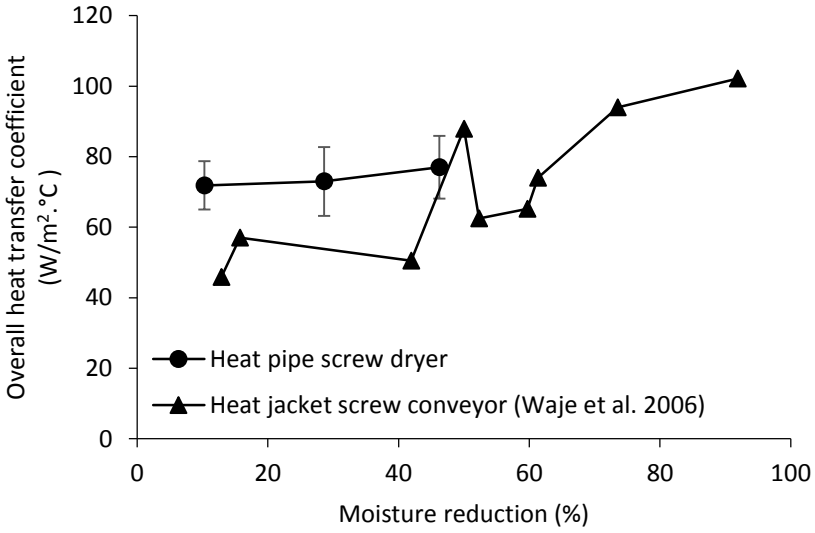

Figure 19. The overall heat transfer coefficient as a function of moisture reduction plotted for the HPSD and a steam-based screw conveyor dryer. Note: no standard deviation data were presented by Waje et al. 2006 [10].

3.3 Outlook on HPSD for ceramic slurry drying

Even with the driest possible product, the quality did not match the granular product of spray dryer (pasty vs. granular). One approach is to compress the product in a roller compactor and subsequently milled through screen downstream of the HPSD so that the product can then be pressed into tiles. The benefit of using HPSD in this manner would only be feasible should these additional unit operations not compromise on the energy already saved by using the HPSD. Various scale up approaches for the HPSD may be considered, including:

- Increasing the screw speed i.e. process-based scale up, but this needs to be done with care i.e. process optimisation must be carried out to ensure conformance with required product moisture content.
- Raw material feed rate can also be increased to increase throughput.
- Parallel HPSDs in operation, employing similar process conditions to provide higher throughputs.
- The heat pipe and screw diameters can be increased to some extent to allow more material to be processed per unit time while still maintaining acceptable heat transfer capacity and energy usage.

To further improve the HPSD design and operation, several measures can be considered for implementation as follows:

- The hollow screw conveyor can be filled with a cylindrical heating element to supplement the heat transfer from the heat pipe as well as to increase the heat transfer area.
- The current clearance between the screw and the barrel of 2.4 mm can be reduced to a minimum e.g. 0.5 mm to scrape the developing fouling layer as the screw rotates. This would also increase its overall heat transfer coefficients as a thermal barrier is removed.

- The ‘Xylan’-coating can be applied to the inner barrel surface, in addition to the screw tested in this study, to reduce fouling which occurred predominantly on this heat transfer interface.
- The HPSD is designed to be flexible in the material handling and therefore it could be well suited for the drying of granular, crystalline or powder-type materials. Also, lower drying temperatures than those tested in this present study are possible for heat sensitive materials typically encountered in food and pharmaceutical processes if a different heat pipe fluid (such as methanol) is employed.

4 Conclusions

In this work, a ‘Heat Pipe Screw Dryer’ (HPSD), a hybrid of the annular heat pipe and screw conveyor technologies was designed and characterised as a novel, continuous and compact dryer for the drying of a ceramic slurry. Under optimised heat pipe operating conditions of 200°C, 11% filling ratio and horizontal orientation, the HPSD was able to reduce the moisture content of the ceramic slurry from 33 wt.% to 18 wt.% at a residence time of 260s (screw speed of 10 rpm). The energy efficiency of moisture removal was 2.04 kg/kWh, which was 3 - 8 times higher than common drying technologies e.g. fluidised beds, rotary and spray dryers, although final product may require further refinement downstream. With the addition of a hot air stream sweep, the final product moisture could be reduced to 7 wt. %, a desired level for direct tile pressing. However, this caused up to 50% reduction in energy efficiency and a very high fouling penalties. Although fouling increased significantly when increasing moisture removal rates, this could be addressed by coating contact surfaces with a non-stick coating material such as the ‘Xylan’ coating tested in this study or by minimising the clearance between the screw conveyor and the barrel surface. With a 35% higher overall heat transfer coefficient than a conventional steam jacketed-screw conveyor dryer, the HPSD offers a feasible opportunity for more efficient heat transfer and drying of a variety of materials in slurry, granular,

crystalline or powder form in a safe and compact device. Further work on residence time distribution of solid in the HDSP is required to establish clear correlations between product properties and operating conditions.

Acknowledgement

The authors would like to thank George Riley and Anna Nicholson for carrying out a major part of the experimentation, Ryan McGlenn and Xiao Yang at Thermacore (Ashington) for the second rig pressure certification and Carmen Segarra at Instituto de Tecnologia Ceramica (Spain) for the tile press and analysis. The authors acknowledge the funding provided by the European Commission under the HORIZON 2020 Programme, for EU Project 680565 – 'Intensified by Design' (IbD).

List of References

1. USDepartmentofEnergy. *Process Heating: Technology Assessment*. 2015 [cited 2017 3 July]; Available from: https://energy.gov/sites/prod/files/2016/06/f32/QTR2015-6I-Process-Heating.pdf.
2. Wang, H., et al., *A review of process intensification applied to solids handling.* Chemical Engineering and Processing: Process Intensification, 2017. **118**: p. 78-107.
3. Tamir, A., *Chapter 7 - HEAT TRANSFER AND DRYING*, in *Impinging-Stream Reactors*. 1994, Elsevier: Amsterdam. p. 227-324.
4. Groenewold, H. and E. Tsotsas, *Drying in fluidized beds with immersed heating elements.* Chemical Engineering Science, 2007. **62**(1): p. 481-502.
5. Torftech. *Sludge processing - drying*. 2016 [cited 2016 31 October]; Available from: http://www.torftech.com/applications/sludge_processing.html.
6. Buss-SMS-Canzler. *Operating Principle of vertical thin film dryers*. 2016 [cited 2016 15 July]; Available from: http://www.sms-vt.com/en/technologies/drying/vertical-thin-film-dryer/operating-principle.html.
7. Waje, S.S., B.N. Thorat, and A.S. Mujumdar, *Screw Conveyor Dryer: Process and Equipment Design.* Drying Technology, 2007. **25**(1): p. 241-247.
8. Khalloufi, S., C. Almeida-Rivera, and A.V. Mudaliar, *Modern Drying Technology, Volume 5: Process Intensification.* Drying Technology, 2014. **32**(16): p. 2017-2020.

9. Euroatomizado, *Work Package 1 Task 1: Definition of process basecase for ceramic processing (Internal report)*, in *Intensified-by-Design an EU Horizon 2020 project*. 2016.

10. Waje, S.S., B.N. Thorat, and A.S. Mujumdar, *An Experimental Study of the Thermal Performance of a Screw Conveyor Dryer.* Drying Technology, 2006. **24**(3): p. 293-301.

11. Kaplan, O. and C. Celik, *Woodchip drying in a screw conveyor dryer.* Journal of Renewable and Sustainable Energy, 2012. **4**(6): p. 063110.

12. Mujumdar, A.S., S.V. Jangam, and H. Osman. *Development of a cost-effective and energy efficient technique for drying Low Rank Coal (LRC)*. 2011 [cited 2017 31 January]; Available from: https://www.arunmujumdar.com/file/group/summary/SCD%20Poster.pdf.

13. Chan, C.W., et al., *Heat utilisation technologies: A critical review of heat pipes.* Renewable and Sustainable Energy Reviews, 2015. **50**: p. 615-627.

14. HeatPipe.nl. *Dutch knowledge center for heat pipe technology*. 2010 [cited 2017 13 December]; Available from: http://www.heatpipe.nl/images/heatpipe.jpg.

15. Thermacore. *Heat Pipe Technology: Passive Heat Transfer for Greater Efficiency*. 2017 [cited 2017 30 July]; Available from: https://www.thermacore.com/thermal-basics/heat-pipe-technology.aspx.

16. Cao, J., et al., *Performance evaluation of controllable separate heat pipes.* Applied Thermal Engineering, 2016. **100**: p. 518-527.

17. Faghri, A., *Review and Advances in Heat Pipe Science and Technology.* Journal of Heat Transfer, 2012. **134**(12): p. 123001-123001-18.

18. Yan, X.K., et al., *Construction of Sodium Heat-Pipe Furnaces and the Isothermal Characteristics of the Furnaces.* International Journal of Thermophysics, 2011. **32**(1): p. 494-504.

19. McDonough, J.R., et al., *Passive isothermalisation of an exothermic reaction in flow using a novel "Heat Pipe Oscillatory Baffled Reactor (HPOBR)".* Chemical Engineering and Processing: Process Intensification, 2016. **110**: p. 201-213.

20. Davis, J.R., *Chapter 1 Introduction to Stainless Steels*, in *Stainless Steels*. 1994, ASM International. p. 9.

21. Reay, D.A., Kew, P. A., *Heat Pipes: Theory, Design and Applications*. Fifth ed. 2006: Elsevier.

22. Van den Hil, M.J. *Screw Heat Exchangers: Thermal Process by Means of Screw Conveyors*. 2017 [cited 2017 3 August]; Available from: www.celsiusprocessing.com/downloads/lezing_bulk_europe.php.

23. ISO. *ISO 18134-3:2015 Solid biofuels -- Determination of moisture content -- Oven dry method -- Part 3: Moisture in general analysis sample*. 2015 [cited 2017 27 May]; Available from: https://www.iso.org/standard/61637.html.

24. Fayed, M.E. and T. Skocir, *Mechanical Conveyors: Selection and Operation*. 1996: CRC Press.

25. Mujumdar, A.S. and T. Kudra, *Advanced Drying Technologies*. Second ed. 2009, Boca Raton Florida: CRC Press.

26. Barua, H., et al., *Effect of Filling Ratio on Heat Transfer Characteristics and Performance of a Closed Loop Pulsating Heat Pipe.* Procedia Engineering, 2013. **56**: p. 88-95.

27. Mozumder, A.K., et al., *Performance of heat pipe for different working fluids and fill ratios.* Journal of Mechanical Engineering, 2012. **41**(2): p. 96-101.

28. Garner, S. *Heat Pipes for Electronics Cooling Applications*. 1996 [cited 2017 14 December]; Available from: https://www.electronics-cooling.com/1996/09/heat-pipes-for-electronics-cooling-applications/.

29. TheEngineeringToolbox. *Specific heat of solids*. 2017 [cited 2017 2 July]; Available from: http://www.engineeringtoolbox.com/specific-heat-solids-d_154.html.

30. MetalCoatings. *Xylan Coatings*. 2011 [cited 2017 30 May]; Available from: http://www.metcoat.com/xylan-coatings.htm.

31. Geeraert, B., *Air drying by heat pumps with special reference to timber drying*, in *Heat Pump and Their Contribution to Energy Conservation*. 1975, NATO Advanced Study Institute, Series E: Applied Sciences: Noordhoff, Leiden. p. 219–246.

32. Alves-Filho, O., *Conventional and Heat Pump Drying: Benefits and Drawbacks*, in *Heat Pump Dryers: Theory, Design and Industrial Applications*. 2015, CRC Press. p. 2-5.

33. Whitford. *Industril coating guide - Xylan*. 2017 [cited 2017 4 July]; Available from: http://www.whitfordww.com/industrial/xylan.html.

34. DuPont. *Teflon PTFE fluoropolymer resin - properties handbook* [cited 2017 3 July]; Available from: http://www.rjchase.com/ptfe_handbook.pdf.

35. Darweesh, H.H.M., *Ceramic Wall and Floor Tiles Containing Local Waste of Cement Kiln Dust-Part II: Dry and Firing Shrinkage as well as Mechanical Properties.* American Journal of Civil Engineering and Architecture, 2016. **4**(2): p. 44-49.

36. Hansen, T. *Firing shrinkage*. 2003 [cited 2017 4 July]; Available from: https://digitalfire.com/4sight/glossary/glossary_firing_shrinkage.html.

37. Nonhebel, G. and A.A.H. Moss, *Drying of Solids in the Chemical Industry*. 1971, London: Butterworth & Co.